FAU–TP3–98/12
CERN–TH/98–232
hep-th/9806231

Transverse Lattice Approach to Light-Front Hamiltonian QCD

S. Dalley[*1] and **B. van de Sande**[**]

[*] *Theory Division, CERN, CH–1211 Geneva 23, Switzerland*

[**] *Institut Für Theoretische Physik III, Staudstraße 7, D–91058 Erlangen, Germany*

Abstract

We describe a non-perturbative procedure for solving from first principles the light-front Hamiltonian problem of $SU(N)$ pure gauge theory in D spacetime dimensions ($D \geq 3$), based on enforcing Lorentz covariance of observables. A transverse lattice regulator and colour-dielectric link fields are employed, together with an associated effective potential. We argue that the light-front vacuum is necessarily trivial for large enough lattice spacing, and clarify why this leads to an Eguchi-Kawai dimensional reduction of observables to $1+1$-dimensions in the $N \to \infty$ limit. The procedure is then tested by explicit calculations for $2+1$-dimensional $SU(\infty)$ gauge theory, within a first approximation to the lattice effective potential. We identify a scaling trajectory which produces Lorentz covariant behaviour for the lightest glueballs. The predicted masses, in units of the measured string tension, are in agreement with recent results from conventional Euclidean lattice simulations. In addition, we obtain the potential between heavy sources and the structure of the glueballs from their light-front wavefunctions. Finally, we briefly discuss the extension of these calculations to $3+1$ dimensions.

[1] On leave from DAMTP, University of Cambridge, Cambridge CB3 0DS, England.

1 Introduction

Light-front Hamiltonian quantisation is a very promising approach to the non-perturbative calculation and understanding of hadronic substructure, as a function of the quark and gluonic degrees of freedom. This is both of intrinsic interest and important for the proper identification of new physics beyond the Standard Model. Recently, we have developed an idea [1], originally suggested by Bardeen and Pearson many years ago [2, 3], for formulating the light-front Hamiltonian of QCD on a transverse lattice. The continuum limit is taken in time and one space direction, while the remaining transverse degrees of freedom are represented as colour-dielectric link variables [4] in a gauge invariant way on the transverse lattice. Since light-front wavefunctions carry the non-perturbative, coherent information about hadronic bound and scattering states in a general Lorentz frame, a solution to this problem would open up a vast amounts of existing and future experimental results to theoretical scrutiny [5]. We believe that the menagerie of light-front Hamiltonian, transverse lattice, and effective colour-dielectric fields, is a very potent combination in the analysis of the strong interactions at intermediate scales. Each contributes to the solution of long-standing technical problems associated with the others. In addition, profound simplifications take place when one considers only the leading order of the $1/N$ expansion [6] in the number of colours N. In this paper, we describe in detail how non-perturbative first principles calculations may be performed for pure gauge theory, in $2+1$ and $3+1$ dimensions, by imposing Lorentz covariance on physical observables. The procedure is then tested with explicit numerical and analytic computations for $2+1$ dimensions at large N, comparing successfully with recent 'state-of-the-art' results on the glueball spectrum from conventional Euclidean lattice simulations, as well as producing many new results.

The choice of dynamical variables and regulator in canonical light-front quantisation is crucial to a practical solution. The well-known Lorentz boost invariance of light-front wavefunctions comes with a price, because, for example, the light-front quantisation surface is not rotationally invariant; typically the regulators chosen will break rotational invariance. An effective potential must be introduced to restore full Lorentz invariance. This effective potential plays another important role to encode what is usually, *id est* in equal-time quantisation, termed 'vacuum structure.' One of the attractive features of light-front quantisation is that, in the true groundstate of a theory, the light-front vacuum is trivial — there can be no pair creation — except possibly for some massless gauge modes of zero momentum. But in the true groundstate, much of the complication usually attributed to the vacuum has only been shifted into effective interactions appearing in the Hamiltonian.

Typically a light-front Hamiltonian will consist of a 'bare' part H_B derived from the classical action, and the effective potential consisting of counterterms H_C. The role of the latter is to enforce

the fundamental (unbroken) symmetries required of the theory, which are broken by the choice of regulators. For practical purposes, one must decide on some physical grounds which subset of all possible operators one is going to consider in H_C, a subset which will then be systematically enlarged as greater accuracy is demanded. The method we will use in our work, to fix the couplings to this subset of operators, is to solve the entire theory as a function of the couplings, which are then tuned by demanding unbroken symmetries of calculated observables. This straightforward approach will allow direct calculations involving typical hadronic scales, intermediate between the asymptotically free region and nuclear scales. Naively, one might think that the approach is computationally unviable, but this is not the case if one uses Hamiltonian methods. There already exists at least one successful application of this approach to fixing counterterms. Parity, which is not a manifest symmetry of the light-front, is typically broken by regulators. Burkardt [7] has shown how, in the case of the Yukawa model in $1+1$ dimensions, a simple counterterm coupling can be adjusted to restore parity invariance in a suitable observable. The general problem in higher dimensions involves the far more complicated task of ensuring the continuous Lorentz symmetries also. This will form the main part of our job in solving pure gauge theory.

To realise the above scenario, we apply light-front quantisation to a set of massive effective degrees of freedom on the transverse lattice — colour-dielectric link variables — which efficiently organise a gauge invariant Hamiltonian in the true vacuum. These variables are supposed to represent an average over the high frequency transverse gluon degrees of freedom. The fact that (lattice) gauge invariance is not broken helps to restrict the number of counterterms needed in H_C, and leads to a simple understanding of confinement. The dielectric variables will provide the required physical basis for systematic approximation to the low-energy effective potential. Moreover, they are flexible enough that in the light-front Hamiltonian formulation one can solve for physical observables, with reasonable computational effort, as a function of the couplings in the effective potential. This formulation therefore satisfies the requirements necessary for our approach. In the first half of this paper, we construct in detail the framework for making calculations in pure gauge theory at large N. This framework is developed in $3+1$ dimensions, but can also be applied in $2+1$ dimensions with some trivial modifications.

As a quantitative test in a highly relativistic, strongly interacting system, we then perform detailed calculations in $2+1$ dimensions. This choice as a testing ground is motivated by a number of reasons. A more reliable computation can be performed in $2+1$ dimensions than $3+1$ dimensions. Teper [8] has recently completed extensive and precise conventional Euclidean lattice Monte Carlo (ELMC) simulations in three dimensions for various N. The resulting spectra may be extrapolated to large N, providing a benchmark for our work. Finally, the physics of Yang-Mills theory in $2+1$

dimensions is remarkably similar that in 3+1 dimensions. In our previous work [1] (hereafter referred to as **I**), we studied the effective potential in $2+1$ dimensions by matching our glueball spectrum to Teper's preliminary data. For a truncated effective potential, we were able to identify a coupling constant trajectory along which mass ratios were approximately constant and agreed reasonably well with the ELMC continuum predictions. This is a perfectly acceptable phenomenological approach, but one would obviously like to avoid fitting to an existing spectrum, whether taken from experiment or another theoretical method. The first principles calculations we perform in this paper use only general concepts like gauge and Lorentz invariance to fix the effective potential. In this way, we can make independent predictions of all physical quantities. The contents of the present paper are summarised below.

In the next section, we briefly review the colour-dielectric formulation of lattice gauge theory and its light-front Hamiltonian limit in order to set notation. In Section 3, we carry out the light-front quantisation, paying particular attention to the interplay of cutoffs, gauge fixing, and energetics. This allows us to show that in the 'colour-dielectric regime' where the light-front Hamiltonian is quantised, light-front zero modes may be neglected, *id est* the light-front vacuum is essentially trivial (this justifies the naive light-front gauge choice often used). We observe that linear confinement is generic to the theory in the colour-dielectric regime. All our work is performed in the large-N limit because of remarkable simplifications which occur. In Ref. [9] and **I** it was proved that, in this limit, one effectively solves the light-front Hamiltonian of a $1+1$-dimensional gauge theory coupled to 2^{D-2} adjoint matter fields, for D space-time dimensions. We clarify in Section 5 the physical role of this Eguchi-Kawai dimensional reduction. Unlike lattice path integral quantisation, where in the leading order in N vacuum structure undergoes dimensional reduction to zero dimensions, the leading order in N of the transverse lattice light-front quantisation exhibits dimensional reduction of physical observables to $1+1$ dimensions. Section 6 outlines procedures for measuring the string tension in the transverse lattice direction via winding modes, and the full spatial potential between two heavy sources, extending work of Ref. [10]. In Section 7, we construct states with nonzero transverse momentum. We use the resulting dispersion relation, together with the string tension measurements, to construct a simple algorithm for fixing the effective potential based on Lorentz covariance.

We then turn to a numerical implementation of our procedure for $2+1$-dimensional gauge theory (Section 8). Most of the relevant formulae and descriptions of our numerical methods have been given in **I**; we review and extend them in Sections 8.1, 8.2, and the Appendices. Section 9 presents our results for the scaling behaviour, glueball masses and wavefunctions, the string tensions and heavy-source potential. Finally, we conclude with a brief discussion of the extension to $3+1$ dimensions

of these calculations.

2 Colour-Dielectric Lattice Gauge Theory.

2.1 Euclidean Lattice

For the purposes of studying a light-front Hamiltonian limit, Wilson's formulation of lattice gauge theory [11] leads to difficulties due to the non-linearity of the link variables [12]. We therefore take as our starting point Mack's linearised 'colour-dielectric' formulation of lattice gauge theory [4]. A similar lattice gauge theory was first introduced by Weingarten [13] as a generator of the spacetime lattice regularisation of the Nambu string action.

On a 4-dimensional hypercubic lattice of spacing a, introduce a complex matrix $M_\mu(x) \in GL(N,C)$ for the link attached to site $x = \{x^0, x^1, x^2, x^3\}$ in the direction x^μ. The partition function is

$$Z = \int \prod_{x,\mu} \prod_{i,j=1}^{N} dM_{\mu,ij}(x)\, dM^*_{\mu,ij}(x)\, \exp(-S[M])\ , \tag{1}$$

with colour indices $i, j \in \{1, \cdots, N\}$ and $M_\mu(x) = M^\dagger_{-\mu}(x + a\widehat{\mu})$. Throughout, $\widehat{\mu}$ is the unit vector in the x^μ direction and $\widehat{-\mu} = -\widehat{\mu}$. For an appropriate choice of action S, this theory is invariant under lattice gauge transformations

$$M_\mu(x) \to U^\dagger(x) M_\mu(x) U(x + a\widehat{\mu})\ , \quad U \in SU(N)\ . \tag{2}$$

Since we will eventually be interested in an expansion of the action in powers of the field M in the large N limit, we take $S[M]$ to consist of Wilson loops and their products. Note that this will include Wilson lines which 'backtrack', such as $\mathrm{Tr}\{M_\mu(x) M^\dagger_\mu(x)\}$, because M is not necessarily a unitary matrix. (Determinants of M are also gauge invariant, but involve an infinite product of fields when $N = \infty$.) Since we are interested in QCD, S is tuned in such a way that, as the correlation length approaches infinity in direction x^μ (lattice spacing $a \to 0$ in physical units),

$$\lim_{a\to 0} M_\mu(x) = 1 + iaA_\mu + O(a^2)\ , \tag{3}$$

where A_μ is the usual hermitian gauge potential. Thus, M must tend asymptotically to the unitary Wilson link variable [11], and in the isotropic continuum limit S will be proportional to $\mathrm{Tr}\{F_{\mu\nu}F^{\mu\nu}\}$. For future reference, it is convenient to introduce lattice versions of the covariant derivative and field strength tensor [4];

$$\overline{D}_\mu M_\nu(x) \equiv M_\mu(x) M_\nu(x + a\widehat{\mu}) - M_\nu(x) M_\mu(x + a\widehat{\nu})\ . \tag{4}$$

This natural definition reduces to $F_{\mu\nu}$ in the continuum.

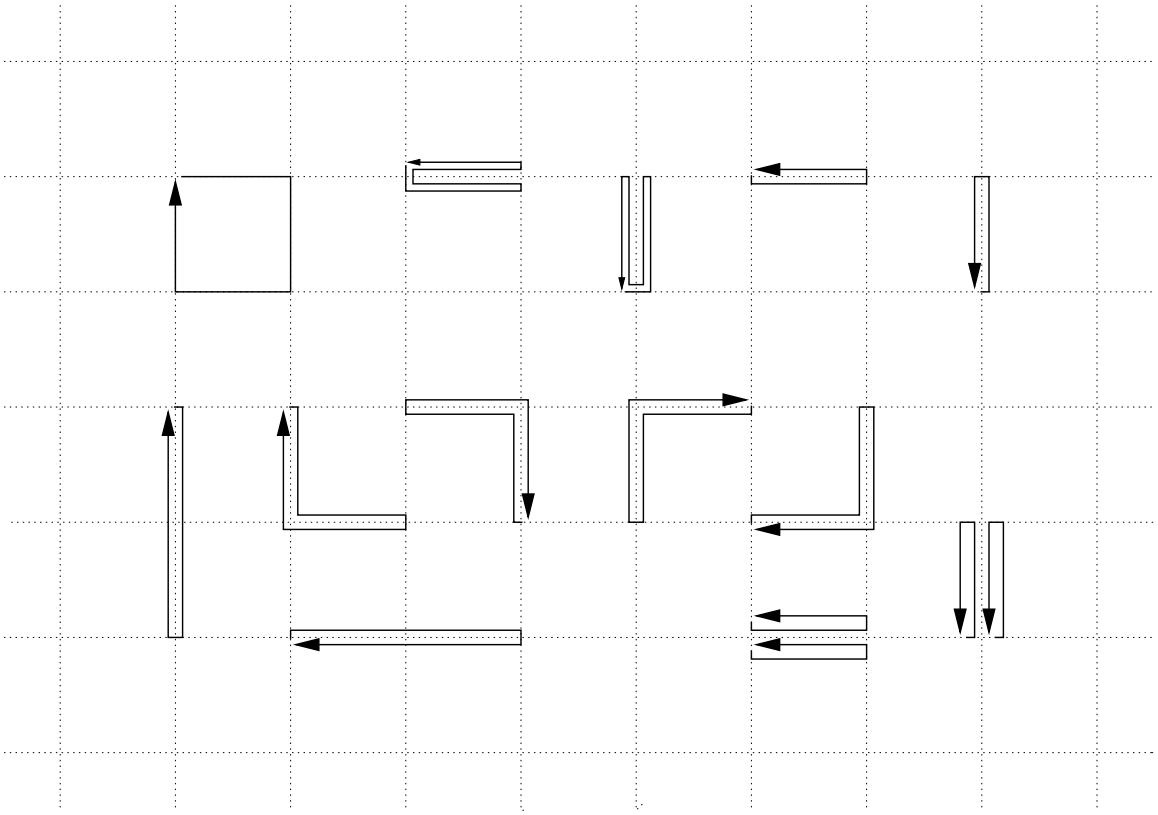

Figure 1: All Wilson loops and their local products of total length ≤ 4. To those shown above one must add the different orientations of each loop in D spacetime dimensions and reversal of arrows (only the plaquette gives a distinct loop in the latter case.) In the case of products of Wilson loops, we have only shown the case where the loops lie exactly on top of one another (local product).

More generally the coefficients of S are to be chosen to obtain scaling, *id est* Green's function observables are to be independent of the correlation length(s). We will demonstrate existence[2] of an approximate scaling trajectory, in the light-front Hamiltonian limit, by demanding Lorentz covariance of boundstate solutions to the theory with S truncated to a finite number of terms. This empirical approach is similar in spirit to the Monte Carlo Renormalisation Group [14]. However, we find it more convenient to directly minimise violations of Lorentz covariance in observables, as a function of couplings in S, rather than try to perform explicit 'block-spin' transformations.

The Wilson loops up to length 4 are illustrated in Fig. 1. The quadratic loop $\mathrm{Tr}\{M_\mu(x)M_\mu^\dagger(x)\}$, *id est* the 'mass squared' term of the $M_\mu(x)$ fields, evidently plays a special role. It must obviously have negative (tachyonic) coefficient in the continuum limit (3). If it has a positive coefficient, a 'strong coupling' expansion of the path integral (1) about $M_\mu(x) = 0$ may be performed [13]. If

[2]Uniqueness would follow from the assumption that the continuum limit of QCD is unique, since the light-front Hamiltonian approach requires us to take the continuum limit (3) in two directions and then demand approximate Lorentz invariance.

the scaling trajectory passes through such a region, Mack showed that a colour-dielectric picture of confinement results [4, 15]. Accordingly, we shall refer to this as the *colour-dielectric regime*. There is evidence for $SU(2)$ that a partition function of the form (1), subject to 'block-spin' transformations, does have renormalisation group trajectories which pass into the colour-dielectric regime at short enough correlation length [16]. Therefore, the picture one should keep in mind is the following. If one decomposes $M_\mu(x) = HU$ into a hermitian matrix H and a unitary matrix U, in the continuum limit $a \to 0$, U is identified with Wilson's link variable. $H = H_0 + \tilde{H}$ gets a VEV H_0, while the fluctuation $\tilde{H}$ becomes very heavy and decouples. Near the continuum limit, H_0 appears in the equations of motion like a generalised dielectric constant [4]. In this regime the field $M_\mu(x)$ is tachyonic. As the lattice spacing a is increased, a scaling trajectory in S pushes one into a region of positive mass squared for $M_\mu(x)$, where H_0 vanishes and $\tilde{H}$ is fully dynamical. The mass of $M_\mu(x)$ then increases with a. We will find further evidence for this in our light-front Hamiltonian calculations later, where it is rather crucial to work in a regime of positive mass squared for $M_\mu(x)$.

2.2 Light-Front Continuum Limit.

It is difficult to perform quantitative calculations with the the dielectric lattice gauge theory described above because one must search the multi-dimensional coupling constant space of S for a scaling trajectory. We will show that these problems can be overcome in the light-front Hamiltonian limit. To employ a light-front Hamiltonian formulation, it is desirable to take the continuum limit in two directions. Thus, in D spacetime dimensions we will take the lattice spacing to zero in the x^0 and x^{D-1} directions while keeping the lattice spacing a in the $D-2$ remaining "transverse" directions constant. Throughout, boldface will denote vectors in the transverse directions, $\mathbf{b}$, with components b^r where $r, s \in \{1, \ldots, D-2\}$. Continuum Lorentz indices are denoted by $\alpha, \beta \in \{0, D-1\}$; thus we write the inner product of two Lorentz vectors as $a^\mu b_\mu = a^\alpha b_\alpha - \mathbf{a} \cdot \mathbf{b}$. Transverse coordinates $\mathbf{x}$ and $\mathbf{y}$ will hereafter be restricted to values corresponding to transverse lattice sites. The covariant derivative (4) in direction x^α becomes

$$\overline{D}_\alpha M_r(\mathbf{x}) = \left(\partial_\alpha + iA_\alpha(\mathbf{x})\right) M_r(\mathbf{x}) - iM_r(\mathbf{x})A_\alpha(\mathbf{x} + a\hat{r}) \,, \tag{5}$$

in the partial continuum limit. One finds a transverse lattice action

$$S = \int dx^0 dx^3 \sum_{\mathbf{x}} \left(\mathrm{Tr}\left\{ \overline{D}_\alpha M_r(\mathbf{x}) \left(\overline{D}^\alpha M_r(\mathbf{x})\right)^\dagger \right\} - \frac{1}{2G^2} \mathrm{Tr}\{F_{\alpha\beta}F^{\alpha\beta}\} - V_{\mathbf{x}}[M] \right) \,, \tag{6}$$

where we have chosen to normalise $M_r(\mathbf{x})$ to have a canonical kinetic term, and repeated indices are summed unless states otherwise. The dimensionful coupling $G^2(a)$ is such that $a^{D-2}G^2 \to g_D^2$ in the classical continuum limit $a \to 0$, where g_D^2 is the continuum gauge coupling in D dimensions.

If we keep only Wilson loops and their products of total length 2 and 4 (which we justify in the next section), the effective potential $V_{\mathbf{x}}$ generically consists of Wilson loops among those shown in Fig. 1, but now understood to be in the remaining $D-2$ dimensional transverse lattice and pinned at one point to $\mathbf{x}$.

The basis (6) for an effective QCD light-front Hamiltonian was earlier proposed in Ref. [2], motivated by considerations of two-dimensional sigma models. Subsequently, an exploratory glueball calculation was performed [3] for some simple choices of V. Those authors speculated that one might be able to find a scaling trajectory in V, corresponding to QCD. We have extended the methods of Ref. [3] in order to answer this question, and perform in this paper quantitative first principles calculations. This allows us to confirm the existence of an approximate scaling trajectory at large transverse lattice spacing (at least in $2+1$ dimensions), and show that it yields the same results for physical observables that are available from conventional methods of studying QCD.

As mentioned above, to take best advantage of the simplifications on the light-front afforded by linear link variables $M_r(\mathbf{x})$, it is quite important to be able to quantise about $M_r(\mathbf{x}) = 0$. Our calculations therefore must implicitly test a light-front Hamiltonian version of the colour-dielectric regime:

In the light-front Hamiltonian limit of lattice action S, we search for a scaling trajectory by canonical quantisation about $M_r(\mathbf{x}) = 0$, taken as the true groundstate.

Once outside of the purported colour-dielectric regime, when a is sufficiently small and $M_r(\mathbf{x}) = 0$ is no longer the minimum of energy, we expect the zero mode structure of light-front quantisation to become much more complicated [17].

3 Canonical Light-Front Quantisation.

3.1 High Energy Cutoffs

We introduce light-front co-ordinates $x^{\pm} = x_{\mp} = (x^0 \pm x^{D-1})/\sqrt{2}$, for all two-vectors in the (x^0, x^{D-1}) plane, and quantise by treating x^+ as canonical time. The variables conjugate to $x^{\pm}$ and $\mathbf{x}$ are $k^{\mp} = (k^0 \mp k^{D-1})/\sqrt{2}$ and $\mathbf{k}$ respectively. Particles and antiparticles have $k^+ \geq 0$. The transverse lattice theory will have divergences associated with the $k^+ \to 0$ limit. This is a high k^- light-front energy limit, as follows from the dispersion relation

$$k^- = \frac{\mu^2 + |\mathbf{k}|^2}{2k^+} \tag{7}$$

for free particles of mass μ. At finite transverse lattice spacing a, this is the only source of divergence, since $\mathbf{k}$ is bounded by the Brillouin zone π/a. In fact, the theory is just a set of coupled $1+1$

dimensional continuum field theories, and there are only the mild free-field divergences characteristic of two-dimensional super-renormalisable theories. For pure gauge theory, finiteness is ensured by a suitable normal-ordering prescription.

At the level of free fields, it follows that if $\mu^2 > 0$ the quantum vacuum is free of particles. Because light-front momentum $k^+ \geq 0$ and is conserved, the zero momentum vacuum state with even one massive ($k^+ = 0$) particle present is infinitely higher in energy than one with no particles. In the interacting theory, the particles must not condense either. In other words, one assumes that one is already expanding about the true vacuum state, and all condensation effects are parameterised by effective interactions in the Hamiltonian. This scenario is precisely realised in the colour-dielectric regime; the dielectric fields $M_r(\mathbf{x})$ are massive and $M_r(\mathbf{x}) = 0$ is the true vacuum. The non-trivial problem is to demonstrate a coupling trajectory in this regime which restores all fundamental (unbroken) symmetries of the theory that have been broken by the regulators.

For fixed total momentum P^+, a large number of particles must carry a very large light-front energy, since each particle is forced to carry a small positive k^+. Although this would also be true of massive particles in an equal-time quantisation, the effect is much more pronounced in the light-front formulation, because of the peculiar inverse relation between momentum and energy (7). In particular, one notes that in the effective potential V, higher powers of the field $M_r(\mathbf{x})$ would couple precisely to those components of the wavefunction with a large number of M-quanta. This is our physical justification for truncation of V to the shortest Wilson loops. Higher loops may be added as greater accuracy is required in the low-energy theory.

There are potentially massless degrees of freedom associated with the continuum fields $A_\pm = (A^0 \pm A^{D-1})/\sqrt{2}$. The behaviour of these modes is subject to the gauge fixing and regulation of the $k^+ = 0$ region, and is discussed in the next section. We will impose periodic boundary conditions in x^- [18], with period $\mathcal{L}$, taking the longitudinal momentum space continuum limit $\mathcal{L} \to \infty$ for fixed a. This gauge-invariant discretisation is also a useful starting point for the numerical investigation of the light-front Hamiltonian [19] (DLCQ).

3.2 Gauge Symmetry

The theory (6) possesses the fields $M_r(x^+, x^-, \mathbf{x})$, $A_+(x^+, x^-, \mathbf{x})$, and $A_-(x^+, x^-, \mathbf{x})$, together with the unitary gauge symmetry at each transverse lattice site $\mathbf{x}$:

$$A_\alpha(\mathbf{x}) \quad \to \quad U(\mathbf{x}) A_\alpha(\mathbf{x}) U^\dagger(\mathbf{x}) + \mathrm{i}\,(\partial_\alpha U(\mathbf{x}))\, U^\dagger(\mathbf{x}) \tag{8}$$

$$M_r(\mathbf{x}) \quad \to \quad U^\dagger(\mathbf{x}) M_r(\mathbf{x}) U(\mathbf{x} + a\hat{r}) \; . \tag{9}$$

The gauge fixing of this theory may be performed following similar treatments in Refs. [20]. With periodic boundary conditions on x^-, we can pick the gauge $\partial_- A_- = 0$. This does not generate a Fadeev-Popov Jacobian since it is (almost) an axial gauge. This leaves the zero modes

$$A^0_-(x^+, \mathbf{x}) \equiv \int_0^{\mathcal{L}} dx^- A_-(x^+, x^-, \mathbf{x}) \; , \tag{10}$$

which may be further gauge fixed to diagonal form

$$A^0_{-ii} \; , \quad i \in \{1, 2, ..., N\} \; , \quad \sum_i A^0_{-ii} = 0 \; , \tag{11}$$

by x^--independent gauge transformations. It is convenient to define

$$c_i = \frac{\mathcal{L}}{2\pi} A^0_{-ii} \; . \tag{12}$$

The gauge fixing to diagonal form (11) generates a Jacobian, which is just the invariant group measure for $SU(N)$, proportional to

$$\prod_{i,j} \left(\sin{(c_i - c_j)\pi}\right)^2 \tag{13}$$

at each site $\mathbf{x}$ on the transverse lattice. This produces a repulsion between the eigenvalues c_i. A_+ will turn out to be a constrained field which may be eliminated by its equation of motion in terms of the $M_r(\mathbf{x})$'s and c_i's.

There are residual global gauge transformations

$$U_{ij} = \delta_{ij} \mathrm{e}^{\mathrm{i}\pi m_i x^-/\mathcal{L}} \quad , \quad \sum_i m_i = 0 \; , \tag{14}$$

where $m_i \in \{\pm 2, \pm 4, ...\}$; c_i transforms as

$$c_i \to c_i - m_i/2 \quad \text{(Gribov)}. \tag{15}$$

This generates Gribov copies. For pure gauge theory there are also the center global gauge transformations for each space direction x^-, $\mathbf{x}$. For x^- they are of the form

$$U_{ij} = \delta_{ij} \mathrm{e}^{\mathrm{i}2\pi x^- n/\mathcal{L}N} \; , \quad i, j < N \; , \tag{16}$$

$$U_{NN} = \mathrm{e}^{-\mathrm{i}2\pi x^-(N-1)/\mathcal{L}N} \; , \tag{17}$$

for $n \in \{1, 2, \cdots, N-1\}$. For $N = \infty$ we can ignore the last matrix element and think of $\exp(2\pi x^- s/\mathcal{L}) \cdot \mathbf{1}$ for $0 < s < 1$. (More generally we will ignore the extra $U(1)$ difference between $SU(\infty)$ and $U(\infty)$ when it does not matter.) c_i transforms as

$$c_i \to c_i - s \quad \text{(Centre)}. \tag{18}$$

In the case that x^1, say, is compactified with period L_1, the center transformations are accordingly $\exp(2\pi \mathrm{i} x^1 s/L_1)\cdot \mathbf{1}$ for $0<s<1$. Under the latter, $M_r(\mathbf{x})$ for $\hat{r}=(1,0)$ transforms as

$$M_r(\mathbf{x}) \to \mathrm{e}^{2\pi \mathrm{i} s a/L_1} M_r(\mathbf{x}) \ . \tag{19}$$

Thus a Polyakov loop (winding mode) $W_{(p,0)}$, of winding number p around L_1, transforms as

$$W_{(p,0)} \to \mathrm{e}^{2\pi \mathrm{i} p s} W_{(p,0)} \ , \tag{20}$$

independent of L_1.

3.3 Confinement and Zero Modes

The final gauge-fixed action is

$$S = S_1 + S_2 + S_3 \ , \tag{21}$$

where

$$\begin{aligned}
S_1 &= \int dx^+ dx^- \sum_{\mathbf{x}} \mathrm{Re}\left[\ \mathrm{Tr}\big\{\partial_+ M_r(\mathbf{x}) \overline{D}_- M_r^\dagger(\mathbf{x})\big\}\right] - V_{\mathbf{x}}[M] && (22)\\
S_2 &= \int dx^+ dx^- \sum_{\mathbf{x}} \frac{1}{G^2}\,\mathrm{Tr}\Big\{\big(D_- A_+(\mathbf{x})\big)^2\Big\} + \ \mathrm{Tr}\ \big\{A_+(\mathbf{x}) J^+(\mathbf{x})\big\} && (23)\\
S_3 &= \int dx^+ \sum_{i,\mathbf{x}} \frac{4\pi^2}{G^2\mathcal{L}} (\partial_+ c_i(\mathbf{x}))^2 && (24)\\
J^+(\mathbf{x}) &= i\Big[M_r(\mathbf{x})\left(\overline{D}_- M_r(\mathbf{x})\right)^\dagger - \left(\overline{D}_- M_r(\mathbf{x})\right) M_r^\dagger(\mathbf{x}) + \\
&\qquad M_r^\dagger(\mathbf{x}-a\hat{r})\overline{D}_- M_r(\mathbf{x}-a\hat{r}) - \left(\overline{D}_- M_r(\mathbf{x}-a\hat{r})\right)^\dagger M_r(\mathbf{x}-a\hat{r})\Big] \ . && (25)
\end{aligned}$$

Here $D_-\phi = \partial_-\phi + \mathrm{i}[A_-,\phi]$. The A_+ constraint equation of motion obtained from S_2 is then

$$\frac{2}{G^2} D_-^2 A_+ = J^+ \ . \tag{26}$$

Formally inverting (26) one derives the longitudinal 'Coulomb' interaction at site $\mathbf{x}$,

$$S_2 = \int dx^+ dx^- \sum_{\mathbf{x}} \frac{G^2}{4}\,\mathrm{Tr}\big\{J^+(\mathbf{x})(D_-)^{-2} J^+(\mathbf{x})\big\} \ . \tag{27}$$

We expect this to produce linear confinement in the longitudinal direction, because of the classical nature of this effect for the two-dimensional gauge theory at each lattice site.

The degrees of freedom c_i are essentially winding modes around $\mathcal{L}$, since

$$\mathrm{Tr}\left\{\mathrm{P}\ \exp\left(i\int_0^{\mathcal{L}} dx^- A_-\right)\right\} = \sum_i \mathrm{e}^{2\pi \mathrm{i} c_i} \tag{28}$$

in the present gauge. Therefore the classical linear confinement in two dimensions should push these modes to infinite energy in the $\mathcal{L} \to \infty$ limit. We can see this more formally in the large-N limit. The Schrödinger representation of the kinetic term S_3 (24),

$$-\frac{G^2\mathcal{L}}{16\pi^2}\frac{d^2}{dc_i^2}\ , \tag{29}$$

evidently demonstrates that the modes c_i become classical at $N = \infty$, since G^2N is held finite. Introducing

$$J^+_{ij}(x^-, \mathbf{x}) = \sum_{n=-\infty}^{\infty} \tilde{J}^+_{ij}(n, \mathbf{x}) \mathrm{e}^{-2\pi i n x^-/\mathcal{L}}\ , \tag{30}$$

the longitudinal interaction (27) becomes[3]

$$G^2\mathcal{L} \sum_{n=-\infty}^{+\infty} \frac{\tilde{J}^+_{ij}(n, \mathbf{x})\tilde{J}^+_{ij}(-n, \mathbf{x})}{(n - c_i + c_j)^2}\ . \tag{31}$$

The residual global gauge invariances, (15) and (18), mean that we can look for the classical minimum configuration in the fundamental domain $0 < c_i < 1$. From (31), we see that if $\tilde{J}^+_{ij}(0, \mathbf{x}) \neq 0$, this term contributes an energy of order $\mathcal{L}$. On the other hand, if $\tilde{J}^+_{ij}(0, \mathbf{x})$ vanishes, say $\tilde{J}^+_{ij}(n, \mathbf{x}) \sim (n/\mathcal{L})^s$, a finite energy is only obtained in the $\mathcal{L} \to \infty$ limit if $s > 1/2$. In this case, only $n \sim O(\mathcal{L})$ contributes to finite energy configurations and the c_i are negligibly small by comparison in the covariant derivative D_-. (States on which $\tilde{J}^+_{ij}(0, \mathbf{x})$ vanishes also produce the necessary factor of N to make matrix elements of (31) finite in the large N limit; see Section 3.5.) This argument treats the currents J^+ as essentially classical sources, and could be upset if quantum fluctuations of $M_r(\mathbf{x})$ led to complete screening of the linear potential (27). Provided no condensation of the field $M_r(\mathbf{x})$ takes place, as is assumed in the colour-dieletric regime, this cannot occur.

The above arguments apparently justify use of the naive light-front gauge $A_- = 0$ in the original work [2, 3]. One possible caveat concerns the $O(\mathcal{L})$ contributions of c_i to the light-front energy, from the longitudinal Coulomb interactions (31) between link variables. Although these are infinite as $\mathcal{L} \to \infty$, as demonstrated above, a principle value prescription operates between Coulomb self-energy and Coulomb exchange at zero k^+ momentum transfer, such that linear divergences cancel. It is plausible that the c_i, being relevant near the zero momentum region, might affect this cancellation in such a way as to alter the residual finite part. Very recently, some numerical evidence for this has been given for scalar $SU(2)$ matter [21] (in the case of $SU(2)$ there is only one value of i). In Appendix A we give an argument which shows that the only effect of the zero modes c_i is to finitely renormalise the link-field mass μ^2 via the singular Coulomb interaction (31). This is of no

[3]The apparent divergence at $n = 0$, $c_i = c_j$, can be avoided by using residual gauge freedom to gauge away $A^0_{+ii}(x^+)$ for each i at a specific light-front time x^+, taken as the initial value surface $x^+ = 0$ on which the constraint equations are solved [20].

consequence for our approach, since μ is a renormalised parameter to be determined by physical measurements anyway. We will therefore proceed by dropping the variables c_i from now on.

The charges $\tilde{J}^+(0,\mathbf{x})$ generate x^--independent gauge transformations before gauge fixing, and the requirement that they vanish for finite energy states is the statement of colour confinement for the transverse lattice formulation at fixed a [3]. The mechanism for the confining linear potential in longitudinal and transverse directions is somewhat different in each case however. For the longitudinal direction it arises as the Coulomb potential (27) for the $1+1$-dimensional gauge field theory at each site $\mathbf{x}$. In the transverse directions it arises through the Wilson-Kogut-Susskind argument for lattice gauge theories [11, 23]. For colour singlet at each $\mathbf{x}$, we must build a colour string with the (massive) $M_r(\mathbf{x})$ link fields, the energy being proportional to the number of links in the string. Note however that the colour singlet requirement came from the continuum longitudinal dynamics. In later sections, we will show how one can verify these intuitive arguments by explicit calculation of the transverse and longitudinal string tensions.

3.4 Energy and Momentum

With the considerations of the last subsection in place, only $M_r(\mathbf{x})$ remains as a physical degree of freedom. We derive the total light-front momentum and energy $P^\mu = \int dx^- \sum_{\mathbf{x}} \theta^{+\mu}$,

$$P^+ = 2\int dx^- \sum_{\mathbf{x},r} \mathrm{Tr}\big\{\partial_- M_r(\mathbf{x})\partial_- M_r(\mathbf{x})^\dagger\big\} \tag{32}$$

$$P^- = \int dx^- \sum_{\mathbf{x}} V_{\mathbf{x}}[M] - \frac{G^2}{4}\left(\mathrm{Tr}\Big\{J^+(\mathbf{x})\frac{1}{\partial_-^2}J^+(\mathbf{x})\Big\} - \frac{1}{N}\mathrm{Tr}\big\{J^+(\mathbf{x})\big\}\,\frac{1}{\partial_-^2}\,\mathrm{Tr}\big\{J^+(\mathbf{x})\big\}\right) \tag{33}$$

with $J^+(\mathbf{x})$ now given by (25) with $\overline{D}_- \to \partial_-$. The $1/N$ correction to the Coulomb term in (33) is necessary at large-N for $SU(N)$ to ensure that the longitudinal gluon A_+, having no colour singlet part, does not couple to gauge singlet states. It will turn out to be important only for two-link states at non-zero transverse momentum $\mathbf{P}$.

Given the absence of modes c_i, we recover the residual local gauge symmetry generated by $\tilde{J}^+(0,\mathbf{x})$

$$M_r(\mathbf{x}) \to U^\dagger(\mathbf{x}) M_r(\mathbf{x}) U(\mathbf{x}+a\hat{r}) \tag{34}$$

with $U(\mathbf{x})$ independent of x^-. Following the discussion of the previous subsection, the light-front energy (33) is not finite unless the associated charge vanishes at each site $\mathbf{x}$: $\tilde{J}^+(0,\mathbf{x}) = 0$. Thus, only states invariant under the residual gauge symmetry (34) will have finite energy.

3.5 Fock Space

We impose canonical commutation relations at $x^+ = 0$

$$\Big[M_{r,ij}(x^-,\mathbf{x}),\big(\partial_- M_{s,kl}(y^-,\mathbf{y})\big)^\dagger\Big] = \frac{1}{2}\delta_{il}\,\delta_{jk}\,\delta(x^- - y^-)\,\delta_{\mathbf{x},\mathbf{y}}\,\delta_{r,s}\ . \tag{35}$$

We work in longitudinal momentum space and transverse position space

$$M_r(x^+=0,x^-,\mathbf{x}) = \frac{1}{\sqrt{4\pi}}\int_0^\infty \frac{dk}{\sqrt{k}}\left(a_{-r}(k,\mathbf{x})\,e^{-ikx^-} + a_r^\dagger(k,\mathbf{x})\,e^{ikx^-}\right)\ , \tag{36}$$

$$\left[a_{\lambda,ij}(k,\mathbf{x}),\Big(a_{\rho,kl}(\tilde{k},\mathbf{y})\Big)^\dagger\right] = \delta_{ik}\,\delta_{jl}\,\delta_{\lambda\rho}\,\delta_{\mathbf{x},\mathbf{y}}\,\delta(k-\tilde{k})\ , \tag{37}$$

$$\Big[a_{\lambda,ij}(k,\mathbf{x}),a_{\rho,kl}(\tilde{k},\mathbf{y})\Big] = 0\ . \tag{38}$$

Here, $(a_{\lambda,ij})^\dagger = (a^\dagger_\lambda)_{ji}$ and $\lambda,\rho \in \{\pm 1,\ldots \pm (D-2)\}$ For clarity, we omit the + superscript on light-front momentum k^+ hereafter. The Fock vacuum $|0\rangle$ satisfies $:P^-:|0\rangle = :P^+:|0\rangle = 0$ and is the physical vacuum. The Fock space operator $a^\dagger_\lambda(k,\mathbf{x})$ creates a mode with longitudinal momentum k on the link emanating from site $\mathbf{x}$ in transverse direction $\widehat{\lambda}$. This Fock space is already diagonal in P^+, and serves as a basis for finding the energy levels of P^-. Since the glueball boundstates do not interact with one another at $N=\infty$, this in turn will diagonalise the invariant mass operator $\mathcal{M}^2 = 2P^+P^- - \mathbf{P}^2$ in the frame $\mathbf{P}=0$.

The combinations singlet under (34) are the 'string' states which form closed flux loops on the transverse lattice, *exempli gratia*

$$\begin{aligned}&\mathrm{Tr}\Big\{a^\dagger_{-1}(k_1,\mathbf{x}+a\widehat{1})\,a^\dagger_2(k_2,\mathbf{x})\,a^\dagger_{-1}(k_3,\mathbf{x}+a\widehat{2})\\ &\quad\cdot\ a^\dagger_{-2}(k_4,\mathbf{x}+a\widehat{2}-a\widehat{1})\,a^\dagger_1(k_5,\mathbf{x}-a\widehat{1})\,a^\dagger_1(k_6,\mathbf{x})\Big\}\,|0\rangle\end{aligned} \tag{39}$$

as illustrated in Fig. 2. The longitudinal momenta k_m are unconstrained except for $k_m > 0$ and conservation, $\sum_{m=1}^6 k_m = P^+$ in the above example.

4 Structure Functions.

A standard gauge invariant definition in the continuum of the gluon distribution function $G(x)$ in a hadron $|\Psi(P^+)\rangle$ is [24]

$$G(x) = \frac{1}{2\pi x P^+}\int dy^-\mathrm{e}^{-\mathrm{i}xP^+y^-}\,\langle\Psi(P^+)|\,F_a^{+r}(0,y^-,\mathbf{0})\,\mathcal{O}_{ab}\,F_b^{+r}(0,0,\mathbf{0})\,|\Psi(P^+)\rangle \tag{40}$$

where $F_a^{\mu\nu}(x^+,x^-,\mathbf{x})$ is the field strength tensor with colour index $a,b,c \in \{1,\ldots,N^2-1\}$ and

$$\mathcal{O} = \mathcal{P}\exp\left(\mathrm{i}\int_0^{y^-} dz^- A_c^+(0,z^-,\mathbf{0})\,t_c\right)\ . \tag{41}$$

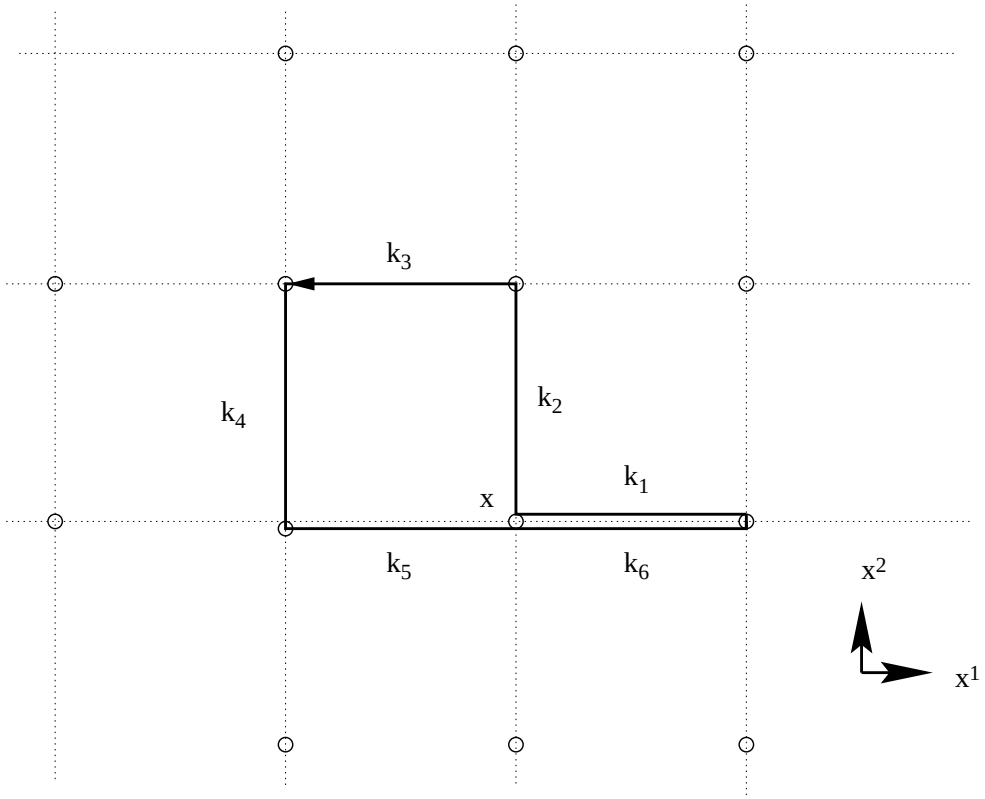

Figure 2: An example of a length 6 loop on the transverse lattice, showing also the longitudinal momentum carried by each link, corresponding to the Fock state (39).

Here, the t_c are the $SU(N)$ generators in the adjoint representation. In the light-front gauge $A_- = 0$ this definition (40) reduces to the expectation value of the gluon number operator. Note that the answer is in fact independent of the choice of $\mathbf{x}$. Since the colour-dielectric formulation deals with a set of collective variables rather than with gluons, the transformation from one to the other being unknown explicitly, we cannot directly measure the gluon distribution. We recall however from (4) and (5) that $\overline{D}_- M_r(\mathbf{x})$ reduces to the field strength F_{-r} in the continuum limit. It seems sensible therefore to make the substitution $F_{-r} \to \overline{D}_- M_r(\mathbf{x})$ in the definition (40). We call the resulting gauge invariant distribution G_d to avoid confusion. In the continuum limit G_d reduces to $G(x)$ but in general they are different. Since $M_r(\mathbf{x})$ are lattice variables, G_d will evolve with the renormalisation scale defined by the edge of the Brillouin zone $\Lambda_\perp = \pi/a$. In the light-front gauge $A_- = 0$ we have

$$G_d(x, \Lambda_\perp) = \frac{1}{2\pi x P^+} \int dy^- \mathrm{e}^{-\mathrm{i}xP^+y^-} \langle \Psi(P^+)| \operatorname{Tr}\{\partial_- M_r \partial_- M_r^\dagger\} |\Psi(P^+)\rangle \tag{42}$$

$$= \langle \Psi(P^+)| a^\dagger_{\lambda,ij}(xP^+, \mathbf{x})\, a_{\lambda,ij}(xP^+, \mathbf{x}) |\Psi(P^+)\rangle \tag{43}$$

Thus G_d has a simple interpretation: the expectation value of the number operator for link fields of longitudinal momentum fraction x. It trivially satisfies the momentum sum rule

$$\int_0^1 dx\; xG_d(x) = 1. \tag{44}$$

and the modes of $M_r(\mathbf{x})$ may be interpreted as 'fat' partons with finite transverse extent. Bjorken scaling violations due to this finite extent will manifest themselves through the evolution with $\Lambda_\perp$ along the scaling trajectory. From the discussion of Section 2.1, one expects the scaling trajectory to pass from large to small values of parton mass μ^2 as the lattice spacing a is reduced. Since a is a measure of the transverse size of the parton, the parton becomes fatter as it becomes heavier. As $\Lambda_\perp$ is increased (a decreased) the glue distribution G_d is expected to evolve to smaller x. This follows simply from the fact that the small x region becomes enhanced the lighter the parton masses, since the free light-front kinetic energy (7) is $\sim \mu^2/x$ for a parton of momentum fraction x. We explicitly calculate structure functions later.

5 The Large-N Limit

In pure gauge theory, the corrections to the large-N limit usually form an asymptotic series in $1/N^2$. For our problem, a dramatic simplification of the relevant Fock space takes place when one neglects these corrections. Firstly, in Ref. [9] and **I** it was shown that in the colour-dielectric regime, the Hilbert space of $\mathbf{P} = 0$ Wilson loops on the transverse lattice, together with the light-front Hamiltonian which acts upon them, undergo dimensional reduction; they may be replaced by an equivalent problem where all links in a given transverse direction are identified. One effectively

works on a transverse lattice with one link in each direction and periodic boundary conditions. This is a manifestation of Eguchi-Kawai reduction [25] in the light-front Hamiltonian framework. One may drop the argument $\mathbf{x}$ in all previous expressions,

$$M_r(x^-, \mathbf{x}) \to M_r(x^-) \quad , \quad a_\lambda(k, \mathbf{x}) \to a_\lambda(k) \; . \tag{45}$$

The proof of the dimensional reduction (45) does not encounter any phenomena analogous to center $U(1)$ breaking [26]; however one must recall that the colour-dielectric regime, on which the proof is based, is only expected at large transverse lattice spacing. In this way, in D spacetime dimensions one ends up having to solve two-dimensional large-N gauge theories coupled to 2^{D-2} complex adjoint scalars. The light-front quantisation of this kind of two-dimensional gauge theory has recently been developed in Refs. [22], whose mathematical analysis we follow closely.[4]

The Hilbert space is further simplified by the fact that the light-front Hamiltonian propagates Wilson loops without splitting or joining at large-N [27]; the amplitude for this is order $1/N$. Thus the light-front Hamiltonian may be studied in the space of connected Wilson loops, that is, states containing one colour trace, *exempli gratia* (39).

The explicit light-front Hamiltonian (33) for the frame $\mathbf{P} = 0$ now becomes equivalently ($D = 4$)

$$\begin{aligned} P^- \;=\; & \int dx^- - \frac{G^2}{4}\,\mathrm{Tr}\Big\{ J^+ \frac{1}{\partial_-^2} J^+ \Big\} \\ & - \frac{\beta}{N a^{D-2}}\,\mathrm{Tr}\Big\{ M_2^\dagger M_1^\dagger M_2 M_1 + \text{hermitian conjugate} \Big\} + \sum_r \mu^2\,\mathrm{Tr}\big\{ M_r M_r^\dagger \big\} \\ & + \sum_r \frac{\lambda_1}{a^{D-2} N}\,\mathrm{Tr}\big\{ M_r M_r^\dagger M_r M_r^\dagger \big\} + \frac{\lambda_2}{a^{D-2} N} \sum_r \mathrm{Tr}\big\{ M_r M_r M_r^\dagger M_r^\dagger \big\} \\ & + \sum_r \frac{\lambda_3}{a^{D-2} N^2} \left(\mathrm{Tr}\big\{ M_r M_r^\dagger \big\} \right)^2 + \frac{\lambda_4}{a^{D-2} N} \sum_{\sigma = \pm 2, \sigma' = \pm 1} \mathrm{Tr}\Big\{ M_\sigma^\dagger M_\sigma M_{\sigma'}^\dagger M_{\sigma'} \Big\} \\ & + \frac{4\lambda_5}{a^{D-2} N^2}\,\mathrm{Tr}\Big\{ M_1 M_1^\dagger \Big\}\,\mathrm{Tr}\Big\{ M_2 M_2^\dagger \Big\} \;, \end{aligned} \tag{46}$$

$$J^+ \;=\; i \Big(M_r \overset{\leftrightarrow}{\partial}_- M_r^\dagger + M_r^\dagger \overset{\leftrightarrow}{\partial}_- M_r \Big) \; . \tag{47}$$

In Section 7.1 we will show how $\mathbf{P} \neq 0$ may be treated in the same dimensionally reduced framework, by adding appropriate phase factors to matrix elements of (46) in the dimensionally reduced Fock basis. We have shown in (46) terms of the effective potential corresponding to Fig. 1 on the transverse lattice, with coefficients $\mu^2, \lambda_1, \lambda_2, \lambda_3, \lambda_4, \lambda_5$, and β. These parameters are to be fixed by a scaling analysis. Note that the multiple Trace operators coupling to λ_3 and λ_5 *do* contribute in leading order of N, but only on 2-parton Fock states. The dimensional reduction in the large-N limit was

[4] The dimensional reduction discussed in those papers, which is an approximation, is not to be confused with the large-N reduction discussed here, which is exact.

not discussed by the authors of Refs. [2, 3], but was used implicitly in the calculations performed there.

The fact, that the large-N limit of the light-front Hamiltonian simplifies the calculations of physical observables in this way is to be contrasted with other quantisation schemes. A path integral evaluation of Green's functions

$$\langle G[A_\mu]\rangle = \int DA_\mu\, G[A_\mu]\, \exp\Big(-\int dx\, S[A_\mu]\Big) \tag{48}$$

should be dominated exactly at $N=\infty$ by an x-independent classical saddle point configuration of the fields A_μ, the 'master field' [28]. This is motivated by the factorisation property

$$\begin{aligned}
&\big\langle\, \mathrm{Tr}\{A_{\mu_1}A_{\mu_2}\cdots A_{\mu_n}\}\ \mathrm{Tr}\big\{A_{\mu_{n+1}}A_{\mu_{n+2}}\cdots A_{\mu_m}\big\}\big\rangle \\
&\quad = \ \langle \mathrm{Tr}\,\{A_{\mu_1}A_{\mu_2}\cdots A_{\mu_n}\}\rangle\ \big\langle\, \mathrm{Tr}\big\{A_{\mu_{n+1}}A_{\mu_{n+2}}\cdots A_{\mu_m}\big\}\big\rangle \\
&\qquad +\frac{1}{N^2}\big\langle\, \mathrm{Tr}\{A_{\mu_1}A_{\mu_2}\cdots A_{\mu_n}\}\ \mathrm{Tr}\big\{A_{\mu_{n+1}}A_{\mu_{n+2}}\cdots A_{\mu_m}\big\}\big\rangle_c
\end{aligned} \tag{49}$$

where $\langle\cdots\rangle_c$ is the connected amplitude. Eqn. (49) can be understood by the usual planar diagram counting rules [6], which attach a factor N^{2-2G-P} to a diagram with G handles and P boundaries. The expectation value of two Wilson loops has a term of order N^2, from the disconnected disks ($P=1$ for each) covering each loop, plus a term of order N^0 from the connected amplitude, the cylinder connecting the two loops. Thus at $N=\infty$, where Eguchi-Kawai reduction in the lattice theory takes place, it appears that one can only calculate disconnected Green's functions and the vacuum energy. In an equal-time Hamiltonian approach, eigenvalues are also dominated by the vacuum contribution of order N^2 (amplitude N to create or annihilate a zero momentum Wilson loop from the vacuum). It is therefore not possible to extract the physical spectrum at $N=\infty$, since this involves contributions down by order $1/N^2$ compared to the vacuum contribution. Physical states interact with the vacuum by emitting or absorbing zero-momentum Wilson loops with amplitude of order N^0 (amplitude $1/N$ to split or join and amplitude N to emit or absorb from the vacuum).

It is then clear why the transverse lattice light-front Hamiltonian framework is uniquely suited for calculations of observables—as opposed to vacuum structure—in the large N limit. The triviality of the light-front vacuum implies that there is no order N^2 contribution. Non-trivial contributions begin at order N^0, corresponding to the free string-like propagation of a Wilson loop. In this way the spectrum of physical states is directly computable at $N=\infty$, where a dimensional reduction in the number of degrees of freedom takes place in the lattice theory. However, unlike the path integral vacuum problem where a reduction to zero dimensions takes place, in the light-front transverse lattice approach dimensional reduction takes place only in the transverse directions. The statement of large-N (Eguchi-Kawai) reduction in D spacetime dimensions for physical observables, rather than

vacuum structure, is that *one can solve for observables in a field theory of $D-2$ fewer dimensions in the large N limit.*

6 String Tensions

6.1 Transverse Tension

To measure the string tension σ_T in the $\mathbf{x} = (x^1, x^2)$ directions, consider a transverse lattice with $\mathbf{n} = (L_1/a, L_2/a)$ links and periodic boundary conditions. We construct a basis of Polyakov loop winding modes in Fock space in the frame $\mathbf{P} = 0$ that wind once around this lattice in both the x^1 and x^2 directions. The shortest such loop has length $|\mathbf{n}|$ in lattice units. One may extract from the lowest invariant mass eigenvalue $\mathcal{M}^2$ the lattice string tension $a\,\sigma_T$ via

$$\mathcal{M}^2 \approx a^2\sigma_T^2\,|\mathbf{n}|^2 \tag{50}$$

for sufficiently large $|\mathbf{n}|$. The form (50) will be imposed as one of the scaling requirements, *id est* σ_T must not to vary with a or direction $\mathbf{n}/|\mathbf{n}|$. Because of large-N reduction, this procedure is equivalent to using Polyakov loops $W_{\mathbf{n}}$ of winding number $\mathbf{n}$, on the transverse lattice with one link in each direction. The total winding number in each direction is conserved due to center symmetry (20). In the large-N limit, we study single Polyakov loops for the same reason that splitting of Wilson loops $W_{(0,0)}$ is suppressed by $1/N$. Thus $\mathbf{n}$ labels disconnected sectors of the Hilbert space.

In sectors of non-zero winding $|\mathbf{n}| \neq 0$, there are further operators one could add to the effective potential $V[M]$ at the same level of approximation. They will in general be necessary for finiteness, as well as to achieve scaling in these sectors. In particular, when the Hamiltonian (46) is put into normal-order, two kinds of quadratic terms are generated, with divergent coefficients c_m and c_w, in the $\mathcal{L} \to \infty$ limit:

$$c_m \int_0^\infty \frac{dk}{k}\,\mathrm{Tr}\Big\{a_\lambda^\dagger(k)a_\lambda(k)\Big\}\,; \tag{51}$$

$$\frac{c_w}{N}\int_0^\infty \frac{dk}{k}\,\mathrm{Tr}\Big\{a_\lambda^\dagger(k)\Big\}\;\mathrm{Tr}\{a_\lambda(k)\}\;. \tag{52}$$

The first (51) is a link-field mass self-energy, and is dealt with by straightforward mass renormalisation, leaving the finite part μ^2. The second (52) is suppressed by $1/N$ on all states except $\mathrm{Tr}\Big\{a_\lambda^\dagger(P^+)\Big\}$, the one-parton state of winding number $\widehat{\lambda}$. To avoid the divergence of the mass of this state, one must add a new counterterm to $V[M]$ given by

$$-\frac{1}{N}\,\mathrm{Tr}\{M_r\}\;\mathrm{Tr}\big\{M_r^\dagger\big\}\;, \tag{53}$$

with an appropriate coefficient to cancel c_w. It is then possible to have a finite part left over, which will appear as a new parameter in the theory. In this case one loses one unit of predictive power

from the measurement of energy levels in the winding number ± 1 sector. Evidently, there are many similar multiple Trace operators one can add to the Hamiltonian, which act in this way on $\mathbf{n} \neq 0$ sectors. They are quite analogous to the multiple trace operators, of which λ_3 is an example (46), which can appear in the $\mathbf{n} = 0$ sector (in that case winding number is conserved 'in each Trace'). However, (53) is the only one required on the grounds of finiteness when the Hamiltonian (46) is put into normal order. In a winding $\mathbf{n}$ sector, multiple Trace operators that contribute in leading order of N must contain at least $\sum_r |n^r|$ powers of $M_r(\mathbf{x})$. Since we try to extract σ_T from large $|\mathbf{n}|$, we will neglect this possible proliferation of parameters to a first approximation, since we neglect higher powers of $M_r(\mathbf{x})$ in the effective potential $V[M]$.

6.2 Heavy Quark Potential

In addition to using Polyakov loops of nonzero winding number in the transverse direction, we can measure the string tension by from the heavy quark potential [10]. The advantage of this approach is that the heavy quark potential can be measured in the x^{D-1} as well as in the transverse directions. The main disadvantage is that this quantity is numerically difficult to compute.

For convenience, we will start with a heavy scalar field $\phi(x^+, x^-, \mathbf{x})$ of mass ρ in the fundamental representation of the colour group (one can just as well start with the Dirac equation and take the heavy limit, the result is the same). In addition to the pure glue 'link-link' interactions, the most general action to fourth order in the fields is

$$\sum_{\mathbf{x}} \int dx^- \, dx^+ \, (D_\alpha \phi)^\dagger \, D^\alpha \phi - \rho^2 \phi^\dagger \phi - \frac{\rho\tau}{a^{D-3}N} \phi^\dagger \left(M_r^\dagger M_r + M_r M_r^\dagger \right) \phi \tag{54}$$

where

$$D_\alpha \phi^\dagger = \partial_\alpha \phi^\dagger - i \phi^\dagger A_\alpha \ . \tag{55}$$

The heavy field contributes to the gauge current J^α in Eqn. (25)

$$J^\alpha_{\text{heavy}} = -i \left(D^\alpha \phi \right) \phi^\dagger + i \phi \left(D^\alpha \phi \right)^\dagger \ ; \tag{56}$$

note that $\phi\phi^\dagger$ is an $N \times N$ colour matrix. Since we are interested in the $\rho \to \infty$ limit, we have not included any hopping terms like $\phi^\dagger(\mathbf{x}) M_r(\mathbf{x}) \phi(\mathbf{x} + a\widehat{r})$ and $\phi(\mathbf{x})$ is pinned to site $\mathbf{x}$ of the lattice. Also, we have not included any "pinching terms" like $\phi^\dagger \phi \phi^\dagger \phi$ which, for large N, acts only on states consisting of two ϕ's.

Now for some kinematics: Let P^α_{full} represent the full 2-momentum of a system containing h heavy particles. It is convenient to split the full momentum into a "heavy" part plus a "residual" part P^α,

$$P^\alpha_{\text{full}} = \rho h v^\alpha + P^\alpha \ , \tag{57}$$

where v^α is the covariant velocity of the heavy quarks, $v^\alpha v_\alpha = 1$. The full invariant mass squared ($\mathbf{P} = 0$) is

$$\mathcal{M}^2 = 2P^+_{\rm full}P^-_{\rm full} = (h\rho)^2 + 2h\rho v^+P^- + 2P^+\left(P^- + h\rho v^-\right) \tag{58}$$

Our choice of v^+ is arbitrary and it is convenient to choose it such that $P^+ = 0$. Consequently, v^+P^- is just the shift of the full invariant mass $\mathcal{M}$ due to the interactions:

$$\mathcal{M} = h\rho + v^+P^- + O\left(1/\rho\right) \ . \tag{59}$$

Thus, v^+P^- is the usual energy associated with the heavy quark potential; this will be our Hamiltonian.

We define creation-annihilation operators associated with the heavy field:

$$\phi = \frac{1}{\sqrt{4\pi}}\int_{-\infty}^{\infty}\frac{dk}{\sqrt{\rho v^+ + k}}\left(b(k)\,{\rm e}^{-iv_\alpha x^\alpha\rho - ikx^-} + d^\dagger(k)\,{\rm e}^{iv_\alpha x^\alpha\rho + ikx^-}\right) \ . \tag{60}$$

The creation/annihilation operators $b(k)$ and $d(k)$ have the usual commutation relations. The ${\rm e}^{i\rho v_\alpha x^\alpha}$ term removes an overall momentum ρv^α from the 2-momentum. The contribution of the heavy particle interactions to the "residual" momenta P^α in Eqns. (32) and (33) are, to leading order in large ρ and N,

$$P^+_{\rm heavy} = \int_{-\infty}^{\infty} dk\,k\left(b^\dagger(k)b(k) + :d(k)d^\dagger(k):\right) \tag{61}$$

$$\begin{aligned} P^-_{\rm heavy} &= -\int_{-\infty}^{\infty} dk\,\frac{k}{2v^{+2}}\left(b^\dagger(k)b(k) + :d(k)d^\dagger(k):\right) \\ &\quad -\frac{G^2}{4\pi}\int dk_1\,dk_2\,dk_3\,dk_4\frac{\delta(k_1+k_2-k_3-k_4)}{(k_1-k_3)^2}b^\dagger(k_1)d^\dagger(k_2)d(k_4)b(k_3) \\ &\quad +\frac{1}{8\pi}\int\frac{dk_1\,dk_2\,dk_3\,dk_4}{\sqrt{k_2k_3}}\left[\delta(k_1+k_2-k_3-k_4)\mathcal{H}_{2\to2}\right. \\ &\qquad \left. +\delta(k_1-k_2-k_3-k_4)\left(\mathcal{H}_{1\to3}+\mathcal{H}_{3\to1}\right)\right] \end{aligned} \tag{62}$$

with

$$\begin{aligned} \mathcal{H}_{2\to2} &= \left(-\frac{G^2\,(k_2+k_3)}{(k_2-k_3)^2} + \frac{\tau}{a^{D-3}N}\right) \\ &\quad \cdot\left(:d(k_1)a_\lambda(k_2)a^\dagger_\lambda(k_3)d^\dagger(k_4): + b^\dagger(k_1)a^\dagger_\lambda(k_2)a_\lambda(k_3)b(k_4)\right) \end{aligned} \tag{63}$$

$$\begin{aligned} \mathcal{H}_{1\to3} &= \left(\frac{G^2\,(k_2-k_3)}{(k_2+k_3)^2} + \frac{\tau}{a^{D-3}N}\right) \\ &\quad \cdot\left(:d(k_1)a^\dagger_\lambda(k_2)a^\dagger_{-\lambda}(k_3)d^\dagger(k_4): + b^\dagger(k_4)a^\dagger_\lambda(k_3)a^\dagger_{-\lambda}(k_2)b(k_1)\right) \end{aligned} \tag{64}$$

$$\mathcal{H}_{3\to1} = \mathcal{H}^\dagger_{1\to3}\,. \tag{65}$$

As an example, let us construct a state with two heavy sources with rest frame separation L in x^{D-1} (this corresponds to an x^- separation of $2v^-L$):

$$|2\rangle = \frac{2\rho v^+}{\sqrt{N}}\int dx^-\,\phi^\dagger\left(x^+, x^- + Lv^-\right)\,\phi\left(x^+, x^- - Lv^-\right)|0\rangle{\rm e}^{-2i\rho v_\alpha x^\alpha} \tag{66}$$

$$= \frac{1}{\sqrt{N}} \int_{-\infty}^{\infty} dk\, b^\dagger(k) d^\dagger(-k) \mathrm{e}^{2iLv^- k} \,. \tag{67}$$

The associated energy shift is

$$\frac{\langle 2|v^+ P^-|2\rangle}{\langle 2|2\rangle} = \frac{G^2 N\,|L|}{4} \,. \tag{68}$$

Thus, as expected, we have linear confinement with string tension of $1/4$ in units of G^2N.

Now, let us investigate the bound state equation for the general case. A state containing two heavy sources with rest frame separation L has the form (suppressing orientation indices λ, ρ):

$$\begin{aligned} |\psi\rangle \;=\; & \sum_p \frac{1}{\sqrt{N^{p+1}}} \int_0^{P^+_{\rm link} < v^+\sqrt{G^2N}P_{\max}} dk_1 \cdots dk_p\, \psi(k_1,\ldots,k_p) \int_{-\infty}^{\infty} dl\, e^{2iLlv^-} \\ & \cdot b^\dagger(l - K/2)\, a^\dagger(k_1) \cdots a^\dagger(k_p)\, d^\dagger(-l - K/2) \end{aligned} \tag{69}$$

where $P^+_{\rm link} = \sum_i k_i$ is the total longitudinal momenta of the link fields. The associated bound state equation has the form:

$$\begin{aligned} P^- v^+ \psi(k_1,\ldots,k_p) \;=\; & \frac{P^+_{\rm link}}{2v^+}\psi(k_1,\ldots) \\ & - \frac{G^2 N v^+}{8\pi} \int \frac{dk'}{\sqrt{k_1 k'}} \frac{k_1 + k'}{(k_1 - k')^2}\, \psi(k', k_2, \ldots)\, e^{iLv^-(k_1 - k')} \\ & + \frac{\tau}{8\pi a^{D-3}} \int \frac{dk'}{\sqrt{k_1 k'}}\, \psi(k', k_2, \ldots)\, e^{iLv^-(k_1 - k')} \\ & + \frac{G^2 N v^+}{8\pi} \int \frac{dk'_1\, dk'_2}{\sqrt{k'_1 k'_2}} \frac{k'_2 - k'_1}{(k'_1 + k'_2)^2}\, \psi(k'_1, k'_2, k_1, \ldots)\, e^{-iLv^-(k'_1 + k'_2)} \\ & + \frac{\tau}{8\pi a^{D-3}} \int \frac{dk'_1\, dk'_2}{\sqrt{k'_1 k'_2}}\, \psi(k'_1, k'_2, k_1, \ldots)\, e^{-iLv^-(k'_1 + k'_2)} \\ & + \frac{G^2 N v^+}{8\pi} \frac{k_2 - k_1}{\sqrt{k_1 k_2}(k_1 + k_2)^2}\, \psi(k_3, \ldots)\, e^{iLv^-(k_1 + k_2)} \\ & + \frac{\tau}{8\pi a^{D-3}} \frac{1}{\sqrt{k_1 k_2}}\, \psi(k_3, \ldots)\, e^{iLv^-(k_1 + k_2)} \\ & + v^+ \text{ (“link-link” interactions from Eqn. (46))} \\ & + \text{“source-link” interactions on the other end of the} \\ & \quad \text{string (complex conjugate of above).} \end{aligned} \tag{70}$$

Note that the first term scales with momentum as $\left(P^+_{\rm link}\right)^1$, the τ terms scale as $\left(P^+_{\rm link}\right)^0$, and all other terms scale as $\left(P^+_{\rm link}\right)^{-1}$. Thus, the longitudinal momentum scale is determined as a balance between the first term and the remaining terms of the Hamiltonian. As opposed to the closed string, an instantaneous-annihilation process via A_+ can act in the $p = 2$ link sector and the “pinching” terms (*exempli gratia* λ_3) do not come into play; otherwise, there are no changes in the “link-link” interactions from the closed string case.

There is a variety of possible cutoffs for k_i that one might choose. The cutoff used here $P^+_{\rm link} < v^+\sqrt{G^2N}P_{\max}$ is convenient because the “link-link” interactions, which act on the interior of the

string, conserve $P^+_{\rm link}$. Holding the other momenta constant and ignoring particle number changing interactions, we see that k_1 has the limiting behaviors[5]

$$\lim_{k_1\to 0}\psi(k_1,\ldots) \quad\propto\quad k_1^\beta\ , \qquad 0<\beta<1/2\ , \quad \frac{\mu^2}{G^2N}=\beta\tan(\pi\beta) \tag{71}$$

$$\lim_{k_1\to \infty}\psi(k_1,\ldots) \quad\propto\quad \left(\frac{\tau}{a^{D-3}k_1^{3/2}}-\frac{G^2Nv^+}{k_1^{5/2}}\right)e^{iLv^-k_1}\ . \tag{72}$$

The first relation is exactly the same "endpoint behavior" that occurs for particles in the interior of the string. The second relation (72) implies that the eigenvalues of v^+P^- converge as $1/\left(P_{\rm max}\right)^5$ for $\tau=0$ and $1/\left(P_{\rm max}\right)^3$ for τ nonzero.

We solve the bound state equation (70) by rescaling and discretising the longitudinal momenta

$$k_i\ \Rightarrow\ \frac{v^+\sqrt{G^2N}P_{\rm max}}{K_{\rm max}}\,\tilde{k}_i\ ,\ \ \tilde{k}_i\in\{1/2,3/2,\ldots\}\ , \tag{73}$$

where $K_{\rm max}\geq K_{\rm link}=\sum_i\tilde{k}_i$ is the maximum total discretised momentum. The ratio $P_{\rm max}/K_{\rm max}$ parametrises the coarseness of the discretization. The discretised bound state equation, expressed in terms of the dimensionless parameters $P_{\rm max}$ and $L\sqrt{G^2N}$, is linear in the couplings

$$\sqrt{G^2N}\ ,\qquad \frac{\mu^2}{\sqrt{G^2N}}\ ,\qquad \frac{\lambda_i}{\sqrt{G^2N}a^{D-2}}\ ,\qquad \frac{\tau}{a^{D-3}} \tag{74}$$

which all have units of mass. For large L, the wavefunction becomes oscillatory. In practice, this forces us to extract the heavy quark potential from relatively small longitudinal separations: of order a few transverse lattice spacings.

7 Lorentz Invariance

One of the advantages of light-front quantisation is that boosts — both longitudinal and transverse — become simple. However, our transverse lattice regulator, along with our use of effective degrees of freedom, break transverse Lorentz covariance. Instead, we will demand Lorentz covariance under transverse boosts for the lightest glueball states; we will use this to help determine the effective potential.

In Section 7.1, we will construct states with nonzero transverse momentum and discuss the associated calculations of eigenstates of P^-. In Section 7.2, we will discuss how these boosted states can be used to help determine the effective potential.

7.1 Non-zero transverse momentum P

For the sake of clarity, we will show the transverse coordinates $\mathbf{x}$ for the link fields $a^\dagger_\lambda(k,\mathbf{x})$. The transverse coordinates will later be dropped: we shall see that non-zero transverse momentum is

[5] The β here is conventional notation for the longitudinal endpoint behavior, not to be confused with the plaquette coupling in (46).

equivalent to introducing various phase factors in the Hamiltonian in the Eguchi-Kawai reduced theory. In the following, we will consider vanishing winding number $\mathbf{n} = 0$; the extension to nonzero winding is discussed in Appendix B.

A generic p-link state of transverse momentum P has the form:

$$\big|\Psi(P^+,\mathbf{P})\big\rangle = \frac{1}{\sqrt{N^p}} \sum_{\mathbf{y}} \mathrm{e}^{i\mathbf{P}\cdot(\mathbf{y}+\bar{\mathbf{x}})}\, \mathrm{Tr}\Big\{ a^\dagger_{\lambda_1}(k_1,\mathbf{x}_1+\mathbf{y})\, a^\dagger_{\lambda_2}(k_2,\mathbf{x}_2+\mathbf{y}) \cdots a^\dagger_{\lambda_p}(k_p,\mathbf{x}_p+\mathbf{y}) \Big\}\, |0\rangle \ . \quad (75)$$

where the winding number vanishes $\sum_{i=1}^p \widehat{\lambda}_i = 0$ and $\mathbf{y}$ is summed over links of the transverse lattice. The transverse coordinates must obey the formula

$$\mathbf{x}_i = \mathbf{x}_{i-1} + a\,\widehat{\lambda}_{i-1} \ , \quad i < 1 \le p \ . \quad (76)$$

Next, we must choose a phase convention for the overall phase $\bar{\mathbf{x}}$ as a function of $\mathbf{x}_1, \mathbf{x}_2, \ldots$. We have found a longitudinal momentum weighted center of mass

$$\bar{\mathbf{x}} = \frac{1}{P^+} \sum_{i=1}^p k_i \left(x_i + \frac{a\,\widehat{\lambda}_i}{2} \right) \quad (77)$$

to be especially convenient. For this choice of $\bar{\mathbf{x}}$, the component M_{-r} of the angular momentum–boost tensor $M_{\mu\nu}$, which generates Lorentz boosts in direction r and obeys

$$[P^-, M_{-r}] = \mathrm{i}P_r \ , \ \ [P^+, M_{-r}] = 0 \ , \ \ [P^r, M_{-s}] = -\mathrm{i}g^r_s P^+ \ , \quad (78)$$

takes on a particularly simple form:

$$\mathrm{e}^{-\mathrm{i}b^r M_{-r}}\, a^\dagger_\lambda(k,\mathbf{x})\, \mathrm{e}^{\mathrm{i}b^r M_{-r}} = a^\dagger_\lambda(k,\mathbf{x})\, \mathrm{e}^{-\mathrm{i}k\mathbf{b}\cdot\mathbf{x}} \quad (79)$$

$$\mathrm{e}^{-\mathrm{i}b^r M_{-r}}\, |\Psi(P^+,\mathbf{P})\rangle = |\Psi(P^+,\mathbf{P}-\mathbf{b}P^+)\rangle \ . \quad (80)$$

In the computation of large-N matrix elements of an operator $\mathcal{O}$

$$\langle\Psi'(P^+,\mathbf{P})|\,\mathcal{O}\,|\Psi(P^+,\mathbf{P})\rangle = \langle\Psi'(P^+,0)|\,\mathrm{e}^{\mathrm{i}P^r M_{-r}/P^+}\,\mathcal{O}\,\mathrm{e}^{-\mathrm{i}P^r M_{-r}/P^+}\,|\Psi(P^+,0)\rangle \ , \quad (81)$$

one obtains phase factors in the Eguchi-Kawai reduced theory. These phase factors correspond to any shift in the weighted center of mass (77). For example, the interaction

$$\mathcal{O} = \sum_{\mathbf{x}} \mathrm{Tr}\Big\{ a^\dagger_{-\lambda}(k_1,\mathbf{x})\, a^\dagger_\lambda(k_2,\mathbf{x}-a\widehat{\lambda})\, a^\dagger_\rho(k_3,\mathbf{x}-a\widehat{\rho})\, a^\dagger_{-\rho}(k_4,\mathbf{x}) \Big\}\, \delta(k_1+k_2-k_3-k_4) \quad (82)$$

picks up the phase factor

$$\mathrm{e}^{\mathrm{i}P^r M_{-r}/P^+}\,\mathcal{O}\,\mathrm{e}^{-\mathrm{i}P^r M_{-r}/P^+} = \mathcal{O}\,\exp\!\left(-\mathrm{i}\,\frac{a(k_1+k_2)}{2P^+}\,\mathbf{P}\cdot\left(\widehat{\lambda}-\widehat{\rho}\right)\right) \ . \quad (83)$$

We can see from this example that the phase factors are functions only of longitudinal momenta and orientation indices λ and ρ. Thus, Eguchi-Kawai reduction of the theory remains.

Although we have constructed states of definite transverse momentum, the construction of the operator $\mathbf{P}$ itself is somewhat problematic. Consider the most natural definition,

$$\mathbf{P} = \frac{i}{2a} \sum_{\mathbf{x},\lambda} \int dk \, \left[a^\dagger_\lambda(k, \mathbf{x} + a\hat{r}) - a^\dagger_\lambda(k, \mathbf{x} - a\hat{r}) \right] a_\lambda(k, \mathbf{x}) \; , \tag{84}$$

which has the correct classical continuum limit. When we apply this operator to a closed colour loop, for example (39), we obtain a state that is no longer a closed colour loop and whose energy therefore diverges. Evidently, the correct form of $\mathbf{P}$ is quite complicated.

In numerical work, it is advantageous to work with a real-valued representation of the Hamiltonian. We note that, in the x^r direction, the boost operator M_{-r} breaks the transverse reflection symmetry $\mathcal{P}^r : x^r \to -x^r$ of the theory. The boost changes sign under transverse reflections,

$$\mathcal{P}^r \, \mathrm{e}^{\mathrm{i}bM_{-r}} \, \mathcal{P}^r = \mathrm{e}^{-\mathrm{i}bM_{-r}} \quad \text{(no sum over } r) \; . \tag{85}$$

For a boost in the x^r direction, we introduce a basis with states that are even and odd under $\mathcal{P}^r$. We use states of the form:

$$|\psi A\rangle \;=\; \cos\left(\frac{P^r M_{-r}}{P^+}\right) (1 + \mathcal{P}^r) \, |\Psi(P^+, 0)\rangle \quad \text{(no sum over } r) \tag{86}$$

$$|\psi B\rangle \;=\; \sin\left(\frac{P^r M_{-r}}{P^+}\right) (1 - \mathcal{P}^r) \, |\Psi(P^+, 0)\rangle \quad \text{(no sum over } r) \tag{87}$$

and the associated phase factors (83) become sines and cosines. The states $|\Psi(P^+, 0)\rangle$ are constructed to have definite charge conjugation $\mathcal{C} \, |\Psi(P^+, 0)\rangle = \pm \, |\Psi(P^+, 0)\rangle$.

7.2 Dispersion Relations.

We now indicate how a scaling analysis can be carried out, by enforcing $SO(3,1)$ Lorentz invariance of physical observables. There are a number of relativistic criterion which one might apply. With only the spectrum of glueball mass ratios, as a function of the couplings in $V[M]$, one might try to obtain Lorentz multiplets. This is a rather narrow test however, since it pays no attention to scalar boundstates. A better measure of relativistic covariance is the glueball dispersion formula. Perfectly relativistic glueballs should satisfy

$$2P^+P^- = \mathcal{M}^2 + |\mathbf{P}|^2 \; . \tag{88}$$

Transverse lattice glueballs will in general satisfy

$$2P^+P^- = G^2N \left(\mathcal{M}_0^2 + \mathcal{M}_1^2 \, a^2 |\mathbf{P}|^2 + \mathcal{M}_2^2 \, a^4 |\mathbf{P}|^4 + \cdots \right) \; . \tag{89}$$

We have used G^2N as the overall scale, so that the measurable coefficients $\mathcal{M}_i^2$ above depend only upon the dimensionless ratios

$$m^2 = \frac{\mu^2}{G^2N} \; , \quad l_i = \frac{\lambda_i}{a^{D-2}G^2N} \; , \quad t = \frac{\tau}{\sqrt{G^2N} a^{D-3}} \; , \quad b = \frac{\beta}{a^{D-2}G^2N} \; . \tag{90}$$

In order that (89) agree with (88) one can tune the couplings so that $\mathcal{M}_2^2 = 0$ and $a^2G^2N\mathcal{M}_1^2 = 1$ for each glueball in the low-lying spectrum. Due to the fact that there are transverse lattice hopping terms in P^-, even when $V = 0$, the dispersion relation automatically becomes asymptotically quadratic for small $a\mathbf{P}$. For this reason, the condition $\mathcal{M}_2^2 = 0$ is more difficult to use to fix V. The condition $a^2G^2N\mathcal{M}_1^2 = 1$, which is more useful, ensures that the speed of light is isotropic. The rotational invariance of the speed of light in the transverse directions was discussed in Ref. [3]. In order to ensure that the speed of light in transverse directions c_T equals that in the x^{D-1} direction c_L (set to one by convention), one must determine the dimensionless combination a^2G^2N.

One way is to measure both the longitudinal and transverse string tensions. This also allows one to express the glueball spectrum in terms of the string tension which is essential for making an absolute prediction of the glueball masses. Suppose we make the following three measurements of dimensionful quantities

$$v_1G^2N = c\sigma \tag{91}$$

$$v_2G^2N = a^2\sigma^2 \tag{92}$$

$$v_3G^2N = \sigma \tag{93}$$

where v_1, v_2, v_3 are measured dimensionless numbers, c is an unknown constant, and σ is the continuum string tension. Eqn. (91) comes from a glueball mass measurement. Eqn. (92) comes from the transverse winding spectrum (Section 6.1). Eqn. (93) comes from the asymptotic heavy-source potential in the x^{D-1} direction (Section 6.2). We have also demanded that the longitudinal and transverse tensions are equal $\sigma_T = \sigma_L = \sigma$. Scaling means that the right hand sides of the above equations are not multiplied by dimensionless functions of a^2G^2N. We now show that this is enough to solve the theory completely.

We use the slope of the dispersion relations at $\mathbf{P} = 0$ for a few low-lying glueballs to estimate the scaling trajectory of V, by demanding isotropy of the speed of light. From (88) and (89) one needs to determine G^2Na^2 in order to compare transverse and longitudinal scales when comparing the speeds of light. From (92) and (93) we can deduce

$$G^2Na^2 = v_2/v_3^2 \tag{94}$$

There are a number of self-consistency checks one can perform, such as examining deviations from quadratic dispersion (non-zero $\mathcal{M}_2^2$), the Lorentz multiplet structure in the glueball spectrum, and rotational invariance of the heavy source potential. Similarly, we can now measure the lattice spacing a and glueball masses c in units of σ.

8 Calculations

We now implement the procedures described in the first half of the paper for the case of $2+1$-dimensional pure large-N gauge theory. The main interest firstly is to compute glueball masses in physical units. These can be compared with results from established techniques to ascertain whether the transverse lattice theory produces correct results, at least to the level of approximation we use. However, it is worth bearing in mind that, apart from confirming known data, the light-front Hamiltonian approach is uniquely suited to the calculation of hadronic wavefunctions in a general Lorentz frame, and it is the latter which chiefly motivates us. We will exhibit the structure of these wavefunctions also. We have also begun analogous calculations in $3+1$ dimensions, which are briefly discussed in the conclusions.

8.1 2+1 Dimensions

Yang-Mills theory in 2+1 dimensions is superrenormalisable. Rather than a logarithmic Coulomb potential, a linearly confining interaction appears to be dynamically generated [8]. Therefore it is rather similar to $3+1$-dimensional QCD. It provides a useful test-bed for non-perturbative calculations, given that two space dimensions can be more efficiently handled numerically than three. The discussion of the first half of the paper can be trivially modified for $2+1$ dimensions (the reader is referred to **I** for further detail). Our light-front Hamiltonian (46) reduces in $2+1$ dimensions to

$$\begin{aligned} P^- &= \int dx^- - \frac{G^2}{4}\,\mathrm{Tr}\Big\{ J^+ \frac{1}{\partial_-^2} J^+ \Big\} + \mu^2\,\mathrm{Tr}\big\{MM^\dagger\big\} \\ &\quad + \frac{\lambda_1}{aN}\,\mathrm{Tr}\big\{MM^\dagger MM^\dagger\big\} + \frac{\lambda_2}{aN}\,\mathrm{Tr}\big\{MMM^\dagger M^\dagger\big\} + \frac{\lambda_3}{aN^2}\left(\mathrm{Tr}\big\{MM^\dagger\big\}\right)^2 \qquad (95) \\ J^+ &= iM \overset{\leftrightarrow}{\partial}_- M^\dagger + M^\dagger \overset{\leftrightarrow}{\partial}_- M \qquad (96) \end{aligned}$$

where now $aG^2 \to g_3^2$ as $a \to 0$, with g_3^2 the standard 2+1 dimensional Yang-Mills coupling in the continuum limit.[6] Otherwise the analysis is unmodified (in particular, the scaling analysis of Sec. 7.2). The link field $M(x^-)$, of course, now points in one transverse direction only. Under large-N reduction it depends only upon x^-, and is equivalent to two real adjoint matrix fields. We are now ready to diagonalise P^- in the Fock space of $M(\mathbf{x})$, as a function of m, l_1, l_2, l_3. G^2N will be used to set the overall scale for dimensionful physical quantities. It will be determined in terms of a physical scale by measurements of the string tension. The glueball spectrum is classified by $|\mathcal{J}|^{\mathcal{P}_1\mathcal{C}}$, for angular momentum $\mathcal{J}$, x^1 reflection symmetry $\mathcal{P}_1$, and charge conjugation $\mathcal{C}$. The latter two are exact while first can only be estimated approximately on the transverse lattice. We follow

[6] In **I**, we did not clearly distinguish between the a-dependent transverse lattice coupling G and the continuum coupling. Moreover, the normalisation of the continuum gauge coupling in that work was nonstandard. Replace G^2 by $2g^2$ and m^2 by $m^2/2$ to convert expressions in this paper to those appearing in **I**.

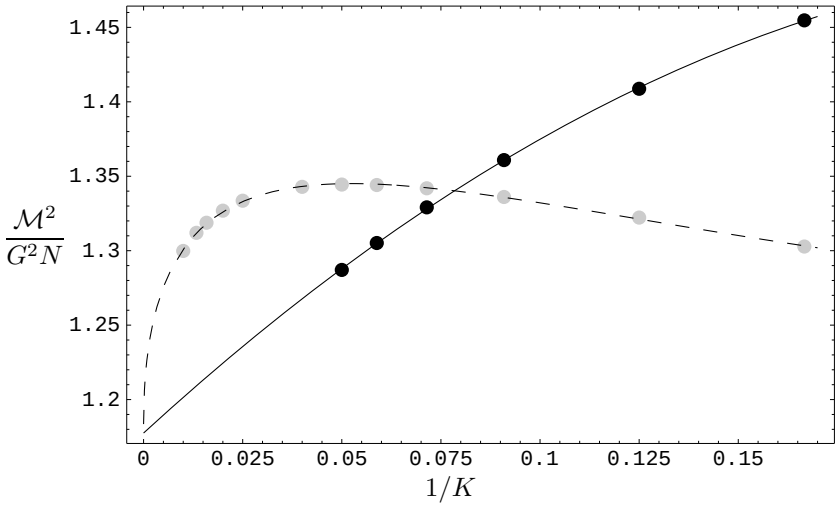

Figure 3: Convergence of the lowest glueball mass as a function of $1/K$ for a 4-link truncation and $\mu^2 = \lambda_i = 0$. The gray points are from conventional DLCQ and the dashed line is a fit to $1.1834 + 1.6395/\sqrt{K} - 5.0731/K + 4.3513/K^{3/2}$. The black points are from a calculation using improved matrix elements and are fit to $1.17752 + 2.44169/K - 4.68183/K^2$. Thus, given data points in the range $10 < K < 20$, the improved matrix elements are necessary for a reliable extrapolation.

the computational methods established in Refs. [22] for adjoint scalar matter in two-dimensions, together with various improvements described in the Appendices of **I** and in the next section.

8.2 Methods

Our basic numerical method is DLCQ [19], where we discretise the longitudinal momentum $P^+ = 2\pi K/\mathcal{L}$ into odd half-integers in the bound state equation. K measures the coarseness of the discretisation and $K \to \infty$ is the longitudinal continuum. This approach has several advantages for numerical work: the resulting Hamiltonian matrix is sparse and matrix elements of the interaction are easy to compute. The main disadvantage of DLCQ is that numerical convergence tends to be slow. In Appendix C of **I**, we introduced an approach which eliminated the most severe convergence problems, the $1/K^{2\beta}$ and $1/\sqrt{K}$ errors, while minimising the remaining $1/K$ error associated with the instantaneous interactions. We have made some subsequent refinements to the method which are described in Appendix C. Because of these improvements, we are able to extrapolate to infinite K with some confidence. For instance, in Figure 3 we plot the eigenvalue of the lowest glueball, calculated using improved matrix elements, as a function of $1/K$. It is clear that a fit to $c_0 + c_1/K$ should work quite well for K between 10 and 20.

In additional to the harmonic resolution K, we truncate the Fock space in the number of links p. We calculate the convergence in p-truncation numerically by looking at the convergence of the lowest eigenvalue for winding number $|\mathbf{n}| = 1$ and $(K, p\text{-truncation}) = (19/2, 3)$, $(25/2, 3)$, $(39/2, 3)$,

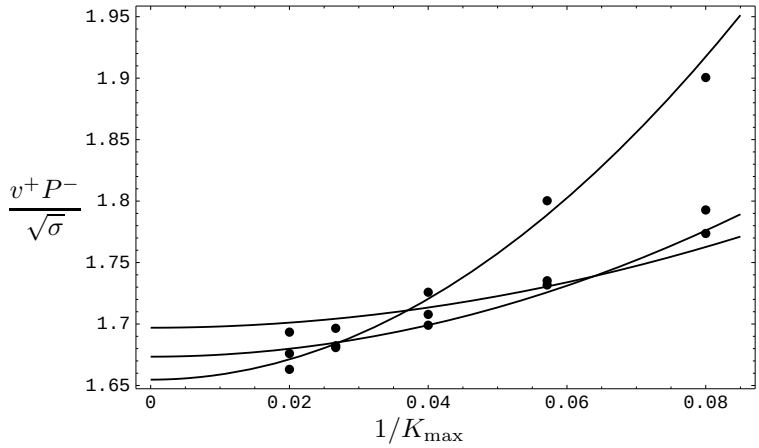

Figure 4: Convergence of the $|\mathbf{n}| = 0$ heavy source potential with $1/K_{\max}$ for $P_{\max} = 4$, 5, 8 and a 2-link truncation. The couplings are from the $m = 0.180255$ datum of Table 1 and the longitudinal separation is $L = 4/\sqrt{G^2N} = 1.750/\sqrt{\sigma}$. The fit function is from Eqn. (99).

$(19/2, 5)$, $(25/2, 5)$, $(23/2, 7)$. Then we fit the eigenvalue to the function

$$c_0 + \left(c_1 + \frac{c_2}{K}\right) \mathrm{e}^{c_p p} + \frac{c_3}{K} \,. \tag{97}$$

It is satisfying that the results for c_p, typically of order -1, agree with the analytic estimate from Appendix B of **I**. We assume that, for sufficiently large p-truncation, c_p is a universal constant; it can be equally well applied to the spectra, nonzero winding $|\mathbf{n}|$, and the heavy source potential.

Using this result for c_p, we calculate spectra for various $(K, p\text{-truncation}) = (18/2, 6)$, $(18/2, 8)$, $(20/2, 6)$, $(20/2, 8)$, $(24/2, 6)$, $(32/2, 6)$ and extrapolate to the continuum using the function

$$c_0 + c_1 \mathrm{e}^{c_p p} + \frac{c_2}{K} \,. \tag{98}$$

We use the same extrapolation procedure for nonzero winding $|\mathbf{n}| \neq 0$. In this case we use $(|\mathbf{n}|, K, p\text{-truncation}) = (2, 20/2, 4)$ $(2, 20/2, 6)$, $(2, 24/2, 4)$, $(2, 28/2, 4)$, $(3, 21/2, 5)$, $(3, 21/2, 7)$, $(3, 23/2, 5)$, $(3, 27/2, 5)$, $(4, 20/2, 6)$, $(4, 20/2, 8)$, $(4, 22/2, 6)$, $(4, 26/2, 6)$. After extrapolating in K and p-truncation using Eqn. (98), we fit the lowest eigenvalue to the form $(\sigma_T a|\mathbf{n}|)^2/(G^2N) + c_1 + c_2/|\mathbf{n}|^2$ as discussed in **I**.

The most tricky calculation is the heavy source potential. Here we have to extrapolate in $K_{\max}$, $P_{\max}$, and p-truncation. In addition, we must choose reasonable values for the longitudinal separation L. For example, in Fig. 4, we see that the eigenvalues are well fit to the function

$$\frac{v^+P^-}{\sqrt{\sigma}} = 1.64873 + \frac{3.08839}{(P_{\max})^3} + 0.64118 \left(\frac{P_{\max}}{K_{\max}}\right)^2 \tag{99}$$

with an RMS deviation of 0.0088. Although we would expect a the leading finite $K_{\max}$ error to be of order $(P_{\max}/K_{\max})^1$, we find the quadratic term to be much more important. Thus, we shall use

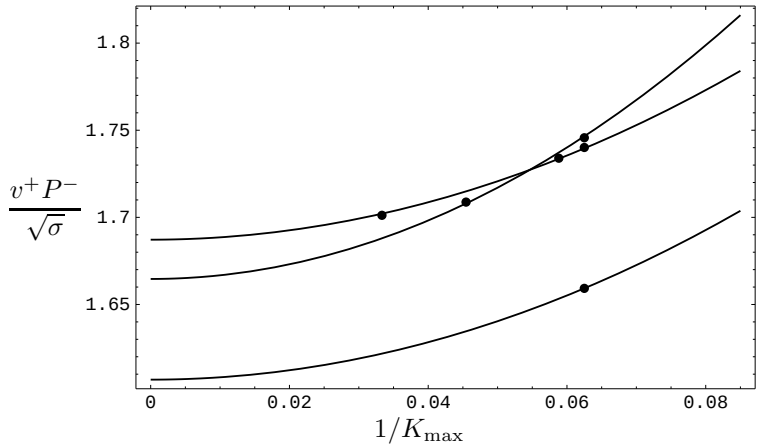

Figure 5: Convergence of the $|\mathbf{n}| = 0$ heavy source potential with $1/K_{\max}$ for various $P_{\max}$ and p-truncations as given by (101). The couplings are from the $m = 0.180255$ datum of Table 1 and $L = 4/\sqrt{G^2N} = 1.750/\sqrt{\sigma}$. The fit function is from Eqn. (102).

the fitting function

$$\frac{v^+P^-}{\sqrt{G^2N}} = c_0 + \frac{c_1}{(P_{\max})^3} + c_2\left(\frac{P_{\max}}{K_{\max}}\right)^2 + c_3\,\mathrm{e}^{c_p p}\,. \tag{100}$$

In subsequent calculations, we fit to (100) using the values

$$\begin{aligned}(|\mathbf{n}|, K_{\max},\, p\text{-truncation}, P_{\max}) = {} & (0, 32/2, 2, 4),\ (0, 32/2, 4, 4),\\ & (0, 32/2, 2, 5),\ (0, 34/2, 2, 4),\ (0, 44/2, 2, 5),\ (0, 60/2, 2, 4),\ (1, 19/2, 3, 4),\\ & (1, 19/2, 5, 4),\ (1, 19/2, 3, 5),\ (1, 33/2, 3, 4),\ (1, 33/2, 3, 5),\ (1, 49/2, 3, 4)\,.\end{aligned} \tag{101}$$

Note that for the heavy source calculation, the conserved quantity $\mathbf{n}$, analogous to winding number, is the number of links minus number of anti-links, *id est* the transverse separation of the sources in lattice units. Example data points are shown in Fig. 5 along with the associated fit function

$$\frac{v^+P^-}{\sqrt{\sigma}} = 1.54997 + \frac{2.95576}{(P_{\max})^3} + 0.838171\left(\frac{P_{\max}}{K_{\max}}\right)^2 + 0.773708\,\mathrm{e}^{c_p p}\,. \tag{102}$$

In order to measure the heavy source potential and test its rotational invariance, we calculate the potential for $|\mathbf{n}| = 0$ and $L\sqrt{G^2N} = 3$, 4, and 6. Then we fit to the functional form [29]

$$\frac{v^+P^-}{\sqrt{G^2N}} = c_0\, L\sqrt{G^2N} + c_1 + \frac{c_2}{L\sqrt{G^2N}}\,. \tag{103}$$

Next we calculate the potential for $|\mathbf{n}| = 1$ and $L\sqrt{G^2N} = 3$; we then demand rotational invariance for this datum.

9 Results

m	l_1	l_2	l_3	t	$\frac{G^2N}{\sigma}$	χ^2	c_p	$\frac{a^2\sigma_T^2}{G^2N}$
0.134186	−0.1263	−0.1178	3.5004	−0.3289	5.3375	17.5267	−1.1680	0.2834
0.180255	−0.0772	−0.2508	221.03	−0.9606	5.2220	12.1472	−1.0791	0.2699
0.227546	−0.1606	−0.1754	7.3792	−1.1712	5.4358	13.6865	−1.1836	0.3473
0.276458	−0.1993	−0.2049	6.4575	−0.9429	5.0986	10.8355	−1.1455	0.3860
0.327475	−0.1783	−0.2133	9.4007	−0.8262	4.6138	12.6389	−1.4465	0.4592
0.381194	−0.2032	−0.1397	3.4963	−1.0544	4.5280	20.9469	−1.7720	0.5671
0.438370	−0.1642	−0.1254	2.0687	−1.2205	4.3206	21.8354	−2.2138	0.6670
0.500000	−0.1731	−0.1284	2.3097	−1.4091	4.1691	22.6331	−2.2572	0.7603

Table 1: The scaling trajectory which minimises the χ^2 test of Lorentz covariance. The couplings l_i, t, and the overall scale G^2N/σ are all obtained from the test. m is equivalent to the lattice spacing degree of freedom.

9.1 First Principles

To search for a scaling trajectory that restores Lorentz covariance, we applied a χ^2 test for certain observables. First, we investigated which observables would be useful in this respect. The natural candidates are the c_T/c_L ratios deduced from glueball dispersion relations, the Lorentz multiplet degeneracy in the spectrum, and rotational invariance of the heavy source potential.

In order to determine which glueballs it makes sense to include in the c_T/c_L part of the χ^2 test, for each low-lying glueball we determined the l_i trajectory such that $c_T/c_L = 1$ for that glueball. In the low-lying spectrum, only the result for the first excited state 0_*^{++} was markedly incompatible with the rest. In fact, it is consistently imaginary. We show below why this artifact is to be expected of our truncation of the effective potential to fourth order. Therefore, excluding this state, we included the c_T/c_L ratio of the lowest seven glueballs: $0^{++}, 2^{++}, 2^{-+}, 0^{--}, 0_*^{--}, 2^{+-}, 2^{--}$. These are the lowest seven glueballs for a broad range of l_i at fixed m, and also the seven lowest in the ELMC simulations [8].

Another possible test of Lorentz covariance is the degeneracy of the parity doublets for the $2^{\pm+}$ and the $2^{\pm-}$. However we find that there is no point in our parameter space where the 2^{++} and the 2^{-+} are degenerate and we do not include this pair in our χ^2 test. For the 2^{+-} and 2^{--}, we have the opposite problem: the two levels are almost degenerate for a vary wide range of couplings. As a consequence, it does not provide a very useful criterion for finding the correct scaling trajectory (although it was included).

In addition, we demand rotational invariance of the heavy source potential based on measurements at $|\mathbf{n}| = 0$ and 1. As described in subsection 7.2, the longitudinal string tension measurement

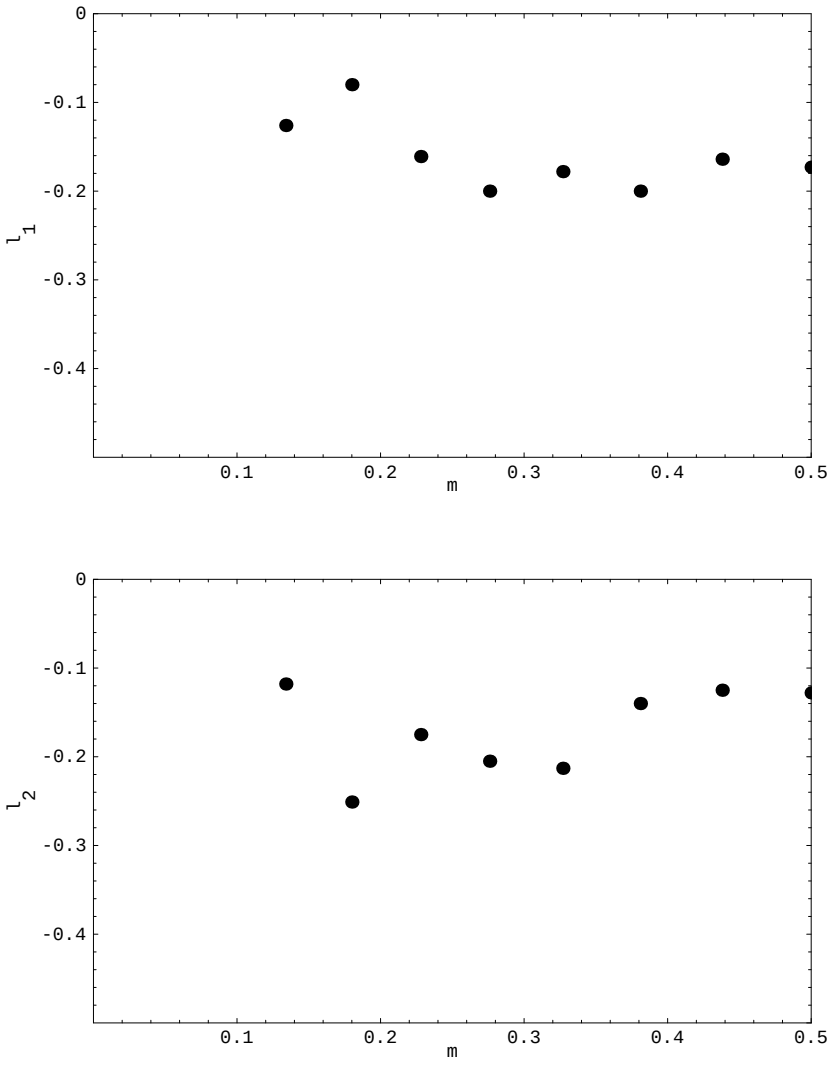

Figure 6: The trajectory which minimises the χ^2 test of Lorentz covariance; see Table 1.

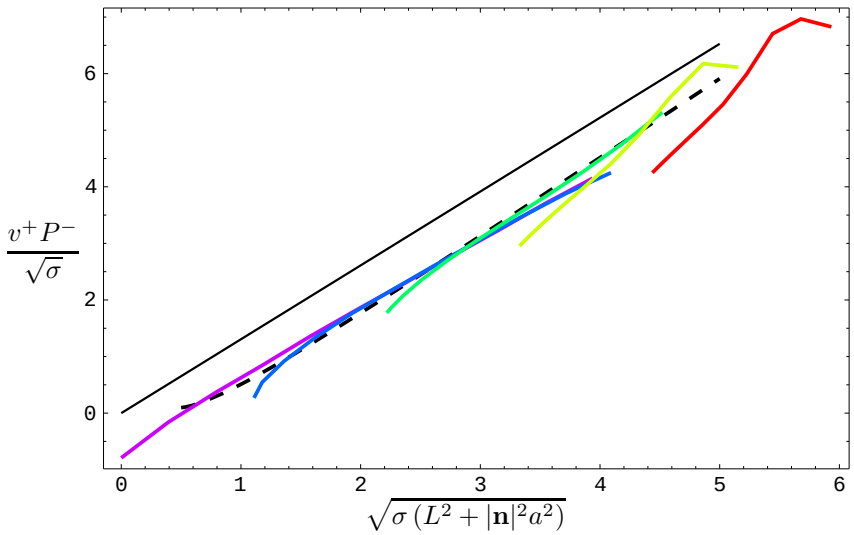

Figure 7: The shaded lines represent the heavy source potential as a function of separation $\sqrt{\sigma\,(L^2+|\mathbf{n}|^2a^2)}$ for $|\mathbf{n}| = 0,\ 1,\ 2,\ 3,\ 4$. The dashed line is from Eqn. (103) and the solid line is the heavy-heavy Coulomb potential from Eqn. (68). The eigenvalues were obtained by extrapolating in $K_{\max}$, $P_{\max}$, and p-truncation; the couplings are from the $m = 0.180255$ datum of Table 1.

determines the overall scale G^2N/σ and, as with our other measurements, we assume that there is some error associated with this. In principle, one might infer the overall scale from demanding consistent dispersion relations of the glueballs, but we found this method to give unreliable results.

The coupling trajectory we find from the resulting χ^2 test is shown in Table 1 and Figure 6. As previously found in **I**, the magnitude of l_3 always comes out much larger than that of l_1 and l_2, essentially infinite. Here we are able to confirm that this is required by Lorentz covariance. We also elaborate on this below. Although there are some fluctuations in the coupling trajectory as m is varied, it is nevertheless remarkably close to the trajectory found in **I** on the basis of a *fit* to the ELMC spectrum.

In determining the trajectory, we inferred roundness of the heavy source potential from measurements at $|\mathbf{n}| = 0$ and 1. If we plot the heavy source potential for more values of $|\mathbf{n}|$, we observe that rotational invariance of the potential is maintained; see Fig 7. A potential that is "oval"—that is, rotationally invariant to within an overall σ_T/σ_L — seems to be generic for the transverse lattice [10]. Consequently, the crucial test is whether one obtains consistent longitudinal versus transverse scales $\sigma_T = \sigma_L = \sigma$.

Examining the glueball masses on this trajectory more closely, we find results for the 0^{++} ground-state mass shown on Figure 8. It is to be anticipated that the χ^2 becomes poor at large and small m. At large m, corresponding to large a (see Fig. 11), the truncated effective potential cannot

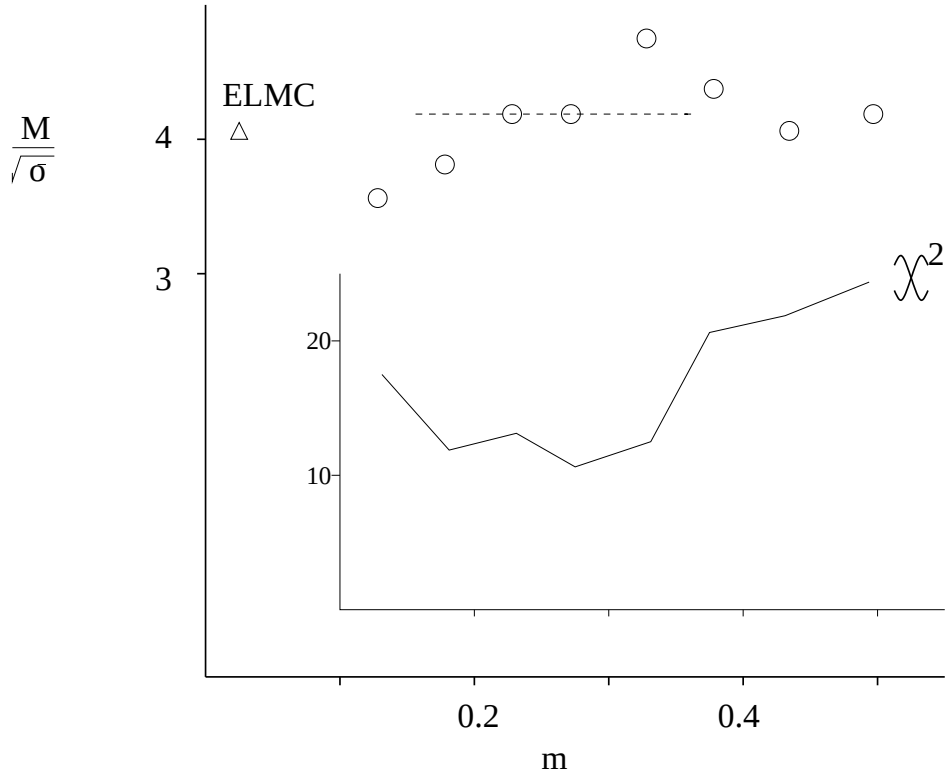

Figure 8: The 0^{++} glueball mass and χ^2 values along the coupling trajectory of Table 1. The size of the data points gives an indication of the error from extrapolation to the longitudinal continuum limit, *id est* the dominant error is from scaling violation on the transverse lattice.

$\lvert\mathcal{J}\rvert^{\mathcal{P}_1 C}$	$M/\sqrt{\sigma}$	c_T/c_L
0^{++}	4.16	1.10
0^{--}	4.86	0.71
2^{++}	5.27	0.59
2^{-+}	6.76	1.00
0^{++}_*	5.39	0.96i
0^{--}_*	6.86	0.87
2^{+-}	7.32	0.39
2^{--}	7.64	0.38

Table 2: The glueball masses at $m = 0.276$ on the scaling trajectory of Table 1 at the minimum $\chi^2 = 10.84$.

cope with the transverse discretisation errors. At small m, the wavefunctions are most sensitive to the the small k^+ region, and hence the longitudinal discretisation errors. It is also the edge of the colour-dielectric regime. The 0^{++} c_T/c_L ratio is 1 ± 0.15 all along the coupling trajectory, and the mass scales to some degree. Based on this, with a generous error for scaling violation, we estimate $M_{0^{++}}/\sqrt{\sigma} = 4.05 \pm 0.3$, in good agreement with the ELMC value[7] $4.08(7)(stat)$.

At the best χ^2, we list the masses and c_T/c_L ratios of the other low-lying glueballs in Table 2. The level ordering of the seven glueballs is in agreement with the ELMC result, and the numerical values are generally not far off. We note however that, with one exception, we cannot get the higher glueballs, along with the string tension and 0^{++}, to be especially rotationally invariant for our approximation to the effective potential. It is perhaps not coincidental that both the masses and c_T/c_L ratios of the higher glueballs come out consistently too low. The one exception, 2^{-+}, is in good agreement with the ELMC mass $6.89(21)(stat)$.

In Figures 9 and 10, we plot the dispersion relation for the 0^{++} and 0^{--} for a point on the scaling trajectory. This is a consistency check, to show whether optimizing the slope at $|\mathbf{P}| = 0$ leads to covariant behaviour throughout the Brillouin zone. Behavior in the figures is generic: the dispersion of the 0^{++} is extremely straight throughout the scaling trajectory and the dispersion of the 0^{--}, along with the other excited states, tend to follow a lattice dispersion $\propto \sqrt{1 - \cos(a|\mathbf{P}|)}$ more closely.

We can also deduce the transverse lattice spacing a in physical units $\sqrt{\sigma}$, as one moves along the trajectory of Table 1 (see Fig. 11). This confirms that the lattice spacing gradually decreases with

[7]The only other accurate value we know of comes from an SU(3) equal-time Hamiltonian lattice calculation [30]. However, apart from $1/N^2$ corrections, it cannot be compared directly with our result since the authors do not measure the string tension, but give results in terms of a gauge coupling.

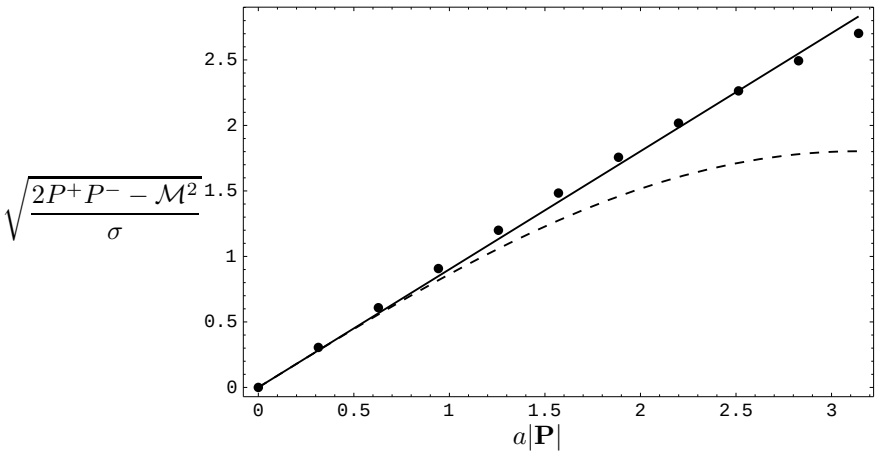

Figure 9: Dispersion relation for the 0^{++} up to the edge of the Brillouin zone. The solid line is the relativistically correct dispersion relation and the dotted line is a lattice dispersion relation. The couplings are from the $m = 0.180255$ datum of Table 1.

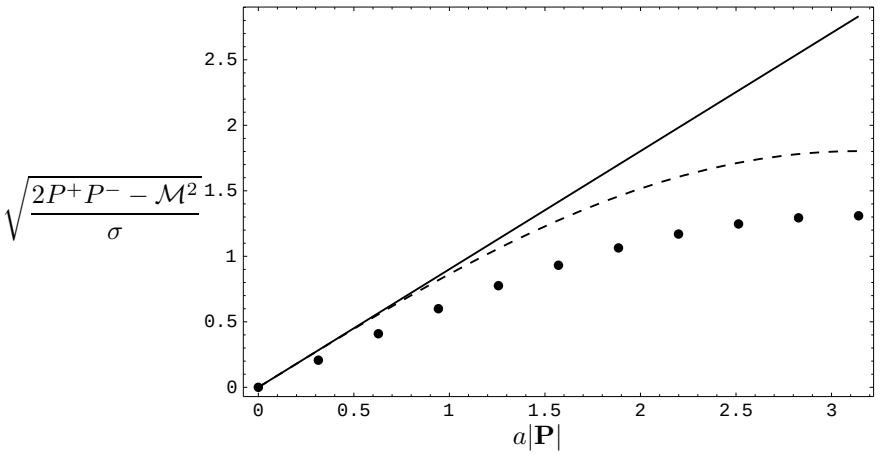

Figure 10: Dispersion relation for the 0^{--} up to the edge of the Brillouin zone. The solid line is the relativistically correct dispersion relation and the dotted line is a lattice dispersion relation (normalised to the same slope at $|\mathbf{P}| = 0$). The 0^{--} typically has a poor slope at $|\mathbf{P}| = 0$ and follows a lattice dispersion more closely. The couplings are from the $m = 0.180255$ datum of Table 1.

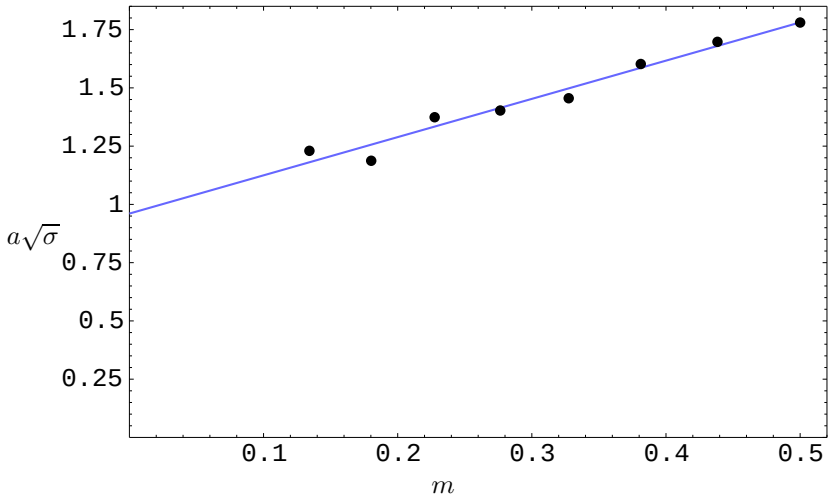

Figure 11: Variation of the lattice spacing a vs. m along the scaling trajectory of Table 1. Also shown is a fit to $0.96 + 1.64m$.

$\lvert\mathcal{J}\rvert^{\mathcal{P}_1\mathcal{C}}$	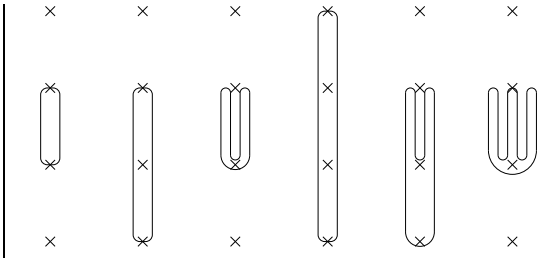					
0^{++}	0.007	0.184	0.676	0.002	0.022	0.108
0^{++}_{*}	0	0.716	0.189	0.009	0.027	0.059
0^{--}	0.889	0.089	0.018	0.001	0.002	0.002
0^{--}_{*}	0.069	0.68	0.118	0.023	0.053	0.056
2^{++}	0.76	0.061	0.14	0.001	0.007	0.03
2^{-+}	0	0.871	0.002	0.005	0.061	0.061

Table 3: The transverse structure of each glueball for $K = 8$, $p \leq 6$, at $m = 0.134$, $l_1 = -0.153$, $l_2 = -0.105$, $l_3 = 100$. Each column shows the probability for a glueball to contain a loop of given transverse shape. Information on the relative phases of different shapes can similarly be obtained from the wavefunctions.

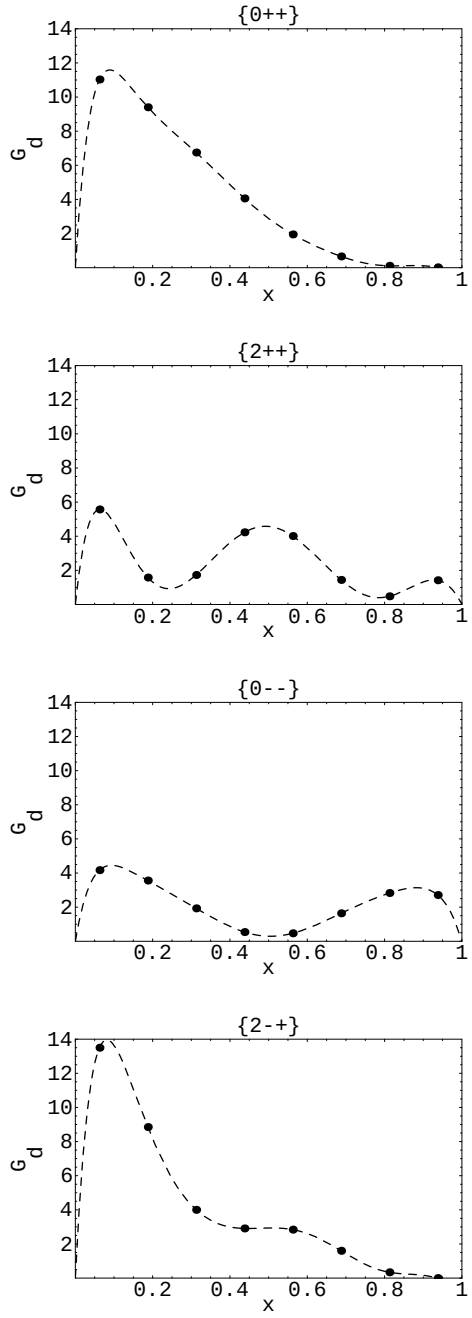

Figure 12: The structure functions $G_d(x)$ for $K = 8$, $p \leq 6$, at $m = 0.134$, $l_1 = -0.153$, $l_2 = -0.105$, $l_3 = 100$. This exhibits the longitudinal structure of each glueball.

m, and is always physically quite large in the colour-dielectric regime $m^2 > 0$. Further information can be gleaned from the glueball wavefunctions, which of course come for free in a Hamiltonian calculation. In Table 3 and Fig. 12 we exhibit the transverse and longitudinal structure of the glueballs at a representative point in coupling space. We see a characteristic rise of the $G_d(x)$-distribution at small x, due to higher Fock states. However, one can show analytically that such distributions must vanish at $x = 0$ for two-dimensional gauge theories [31] (without Yukawa interactions), and therefore our colour dielectric regime $m^2 > 0$ in particular.

The coupling l_3, according to the test for Lorentz covariance, is much larger than other couplings, which might appear unnatural at first sight. However the corresponding operator is also distinguished by the fact that at large N it couples only to link–anti-link Fock states (it 'pinches' the flux tube swept out light-front time x^+). More precisely, if the link–anti-link wavefunction is $f(k^+, P^+ - k^+)$, the l_3 operator has expectation value

$$\langle (\,\mathrm{Tr}\{MM^\dagger\})^2\rangle \propto \left(\int_0^{P^+} dk^+ \frac{f(k^+, P^+ - k^+)}{\sqrt{k^+(P^+ - k^+)}}\right)^2 \tag{104}$$

A complete set of link–anti-link wavefunctions f resulting from the longitudinal Coulomb interaction can be labelled by the number of zeroes of f [2]. The energy increases with the number of zeroes, and one might naively expect the 0^{++} glueball to therefore be predominantly composed of a constant two-link wavefunction. However, this wavefunction and only this wavefunction makes a significant contribution to (104). A large l_3 therefore removes it from all low-lying glueballs, as is evidenced from Table 3 and fig. 12. An intuitive explanation for this follows from the fact that a wavefunction constant in k^+ implies tight binding in the longitudinal direction. On the other hand, the link–anti-link state has width a in the transverse direction. From Fig. 11 we know this to be physically quite large (of order the glueball width!). Therefore it is perhaps not surprising that the Lorentz covariance conditions reject such an asymmetrical Fock wavefunction in low-lying glueballs. If this conclusion carries over to $3 + 1$ dimensions, it will result in a quite different picture from the one suggested in Ref. [3] (which did not include a l_3 coupling).

The absence of the link–anti-link state means that the 0^{++} groundstate glueball is predominantly formed from a linear combination of the 4-link operators $\mathcal{O}_1 = \mathrm{Tr}\{M^\dagger M M^\dagger M\}$ and $\mathcal{O}_2 = \mathrm{Tr}\{MMM^\dagger M^\dagger\}$. In fact, we find that the $(0^{++}, 0^{++}_*)$ system is to a good approximation described by the symmetric and antisymmetric combinations $(\alpha\mathcal{O}_1 + \beta\mathcal{O}_2, \alpha\mathcal{O}_1 - \beta\mathcal{O}_2)$. The operator $\mathcal{O}_2$ couples to $l_2 < 0$ in the Hamiltonian and is the most significant hopping term on the transverse lattice. As a result, we find the symmetric combination lower in energy and with correct relativistic dispersion $c_T^2 > 0$. It then follows unavoidably that the higher-energy anti-symmetric combination will have an incorrect dispersion $c_T^2 < 0$. Since we tentatively identified the anti-symmetric com-

bination with the 0_*^{++}, this explains why we always have a problem with this state. In fact, it is almost purely lattice artifact at present. It is likely that the effective potential must be extended to 6-link operators before this problem can be resolved.

9.2 Improving Higher Glueballs

We have found in the previous section that, determining the glueball masses in terms of a scale set by the rotationally invariant string tension(s), we can obtain a reasonable groundstate 0^{++}, but cannot obtain Lorentz covariant higher glueballs in general. We attribute this incompatibility to our truncation of the effective potential. It is natural to ask if one could find a coupling trajectory which improves the Lorentz covariance of higher glueballs at the expense of rotational invariance of the string tension. In particular, the longitudinal string tension is by far the most difficult measurement we make, and a potential source of systematic errors. To this end, we searched for such a trajectory, using the ELMC value of $M_{0^{++}}/\sqrt{\sigma}$ as a phenomenological input to set the scale. σ was identified with σ_T in this case. Although no longer quite a first principles calculation, the results are sufficiently impressive, we feel, to display here.

Using a χ^2 criterion which includes only the c_T/c_L ratio of the 0^{++} (whose mass is now fixed) and the 0^{--}, we found the trajectory displayed in Fig. 13. In fact, along this trajectory not only are these two glueballs rotationally invariant, but a number of others also have a good c_T/c_L ratio. The trajectory is close to the previous one, but rather more stable. The scaling behaviour of glueball masses, shown in Fig. 14, is also more stable. At the point of minimum χ^2 on this trajectory, we find the spectrum displayed in Fig. 15. In particular, it is worth noting that those glueballs whose c_T/c_L ratio is close to one have predicted masses in agreement with the ELMC result. This encourages us that, by adding further couplings to the effective potential to improve the Lorentz covariance of higher glueballs (from first principles), should bring their masses into line also.

10 Conclusions.

We have constructed an effective transverse lattice light-front Hamiltonian of pure gauge theory, extending the discussion of quantisation and the large-N limit addressed in the earlier works [1, 2, 3], and outlined a first-principles procedure for solving the eigenvalue problem. Not only does this formulation of gauge theory possess the usual appealing features associated with light-front quantisation — trivial vacuum, boost invariance, parton dynamics — but it also efficiently deals with the common problems found in this approach — zero modes, renormalisation, non-compactness/gauge invariance. It does this at the price of introducing an effective potential which must be tuned by demanding Lorentz covariance of eigenstates of the light-front Hamiltonian at large transverse lattice

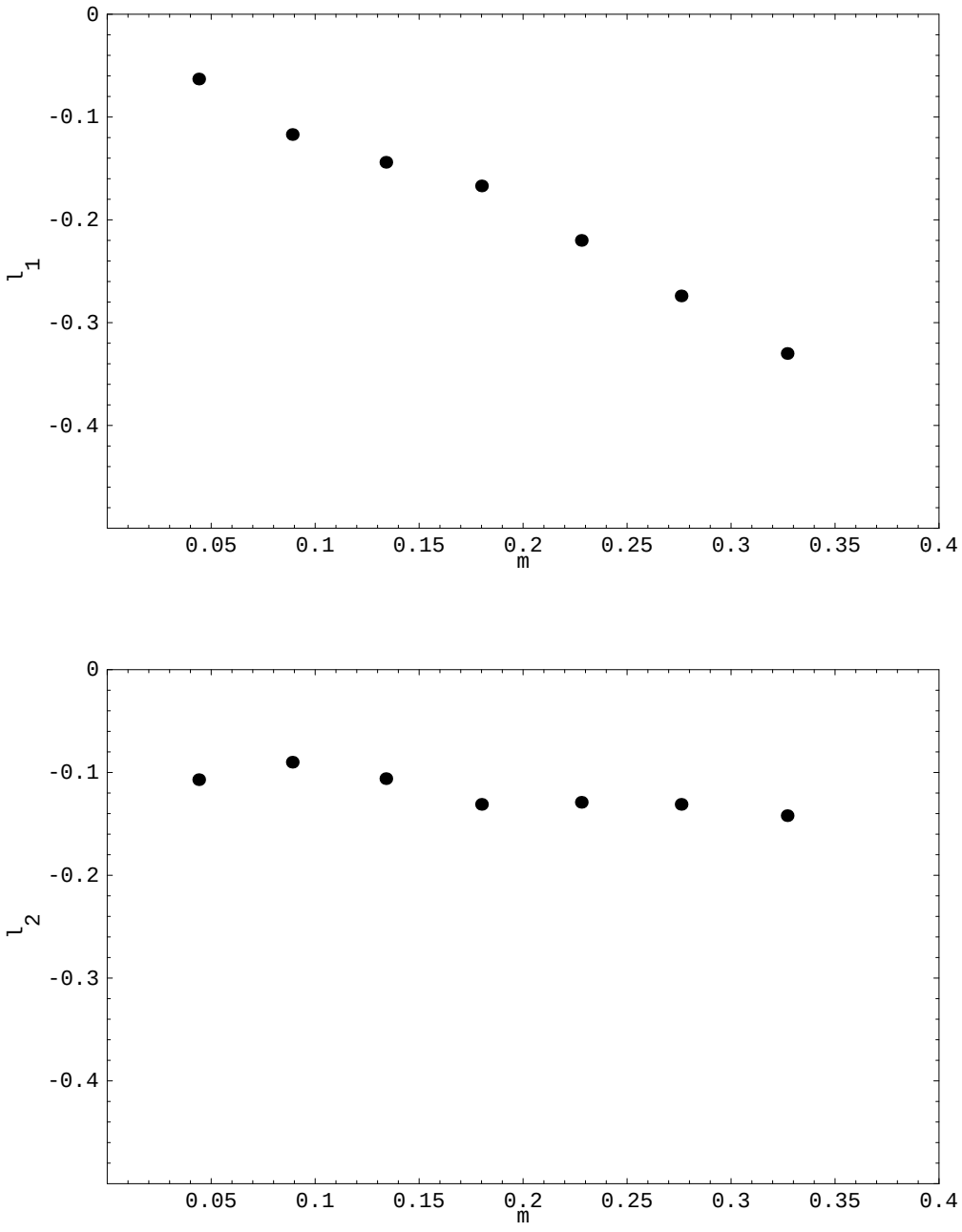

Figure 13: The trajectory which minimises the χ^2 test of Lorentz invariance involving only glueball dispersion formulae.

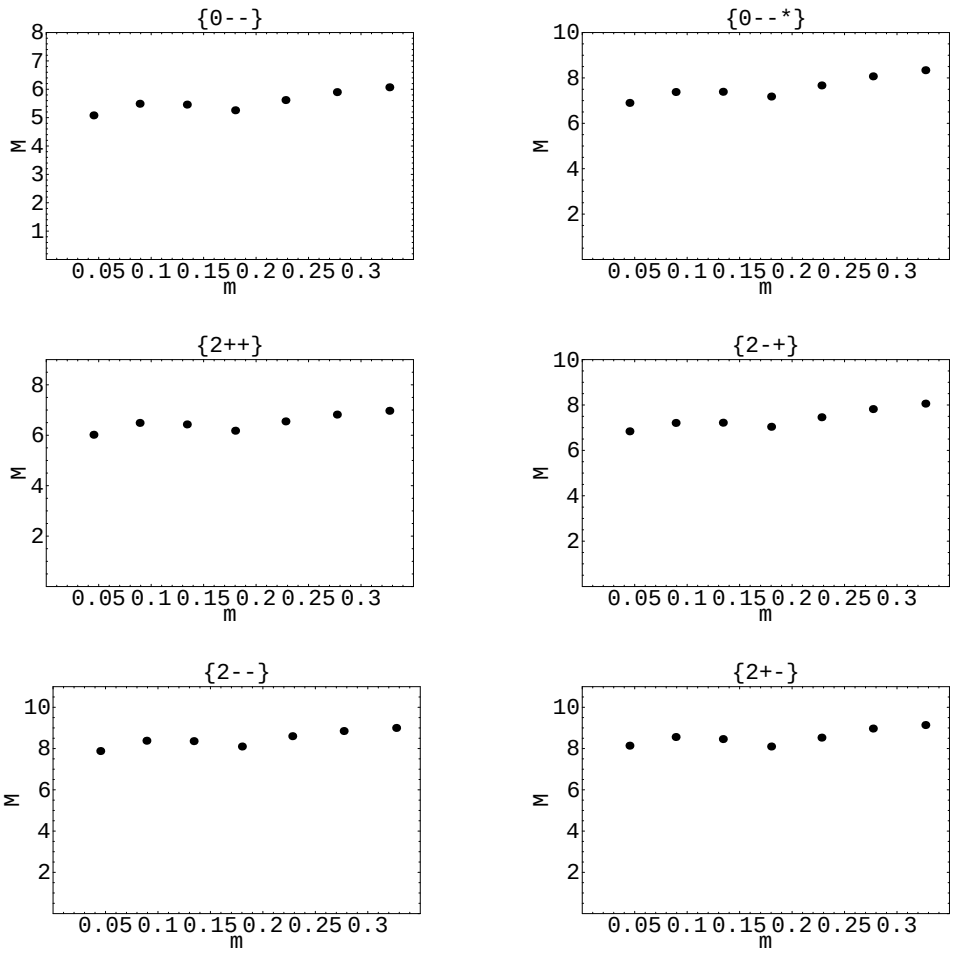

Figure 14: Scaling of the higher glueball masses $\mathcal{M}$ in units of $\sqrt{\sigma}$, as m is varied along the scaling trajectory of Fig. 13. This gives an estimate of systematic errors for each glueball from truncation of V.

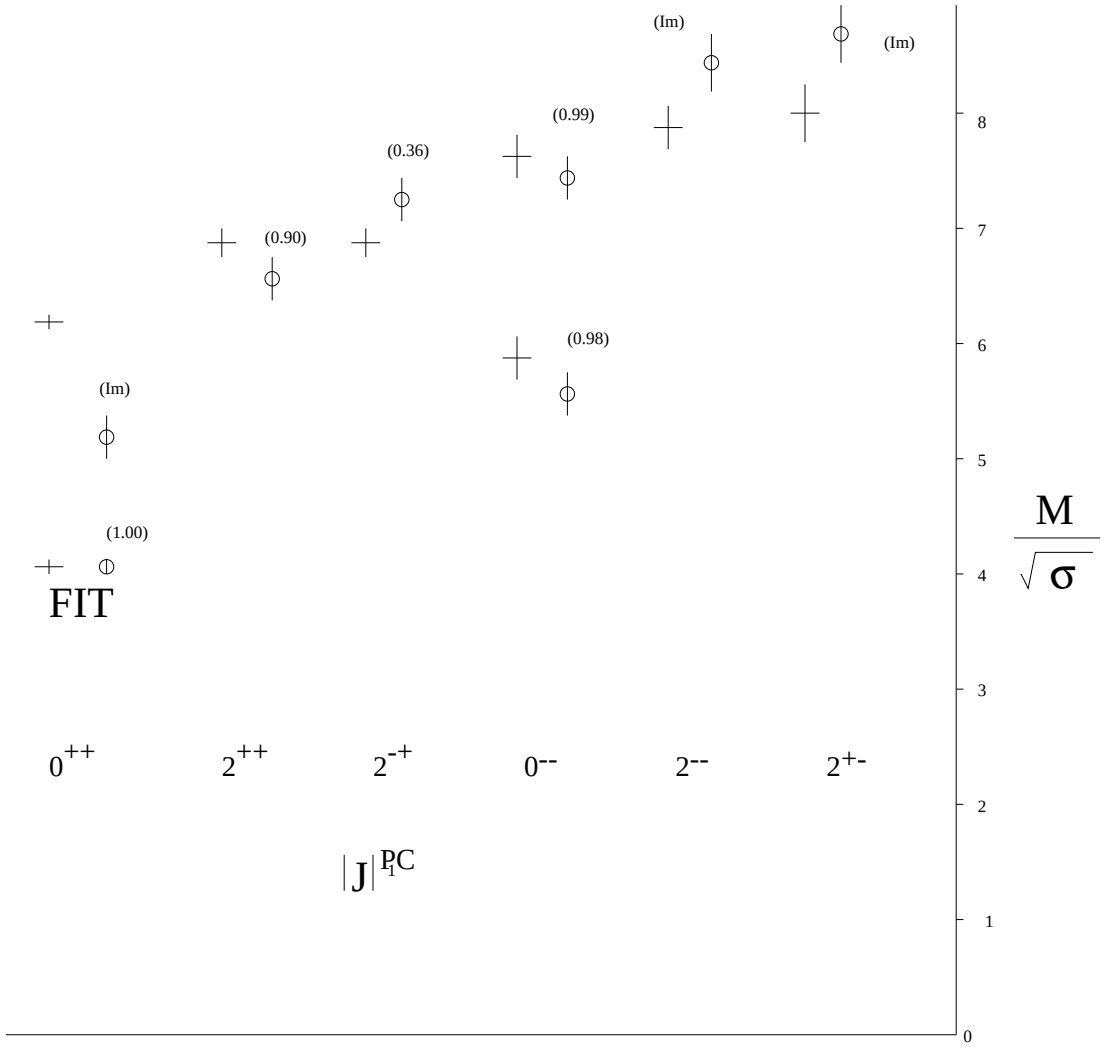

Figure 15: The low-lying $2+1$-dimensional large N glueball spectrum obtained on the transverse lattice (o). Also shown for comparison, the ELMC simulations of Teper (+), extrapolated to $N=\infty$ by a fit to $A+B/N^2$, with statistical errors [8]. The value of $M_{0^{++}}/\sqrt{\sigma}$ was fit to the ELMC result, to set the scale. The other masses result from requiring rotationally invariant dispersion, quantified by the speed of light ratio c_T/c_L deduced from each glueball (in brackets). The estimated error from extrapolation in K and p is shown but an estimate of systematic error from truncation of V is not shown (see Fig. 14).

spacing. Further remarkable simplifications occur in the large N limit. Only a $1+1$ dimensional theory of connected Wilson loops needs to be solved. Equivalently, one solves a $1+1$ dimensional continuum gauge theory coupled to complex adjoint matter fields which form freely propagating colour strings.

We successfully tested the ideas by performing comprehensive calculations in $2+1$ dimensions at large N, using an improvement scheme to extrapolate to the longitudinal continuum limit. We found agreement with conventional Euclidean lattice simulations [8], in those observables for which Lorentz covariance was attained. Furthermore, we could go beyond the path integral approach by obtaining the frame-invariant glueball wavefunctions. Given that the quantisation, regulators, elementary fields, and gauge fixing are different from those of Ref. [8], the agreement is quite impressive. It non-perturbatively validates both the lattice colour-dielectric formulation and the light-front Hamiltonian quantisation of non-Abelian gauge theory at the quantitative level. This is therefore an important step in the application of light-front quantisation to hadronic physics in general.

The obvious extension of large-N pure glue calculations to $3+1$ dimensions has already begun, and initial results are encouraging. For couplings in the light-front Hamiltonian (46) similar to those found for the $2+1$ problem, we find $0^{++}, 2^{++}$, and 1^{+-} multiplets as the lightest glueballs (only some of the components of these multiplets were found in the original work [3]). A search of the full parameter space for a scaling trajectory will yield estimates of the masses and wavefunctions. Given that $1/N^2$ corrections are expected to be smaller than other systematic errors, the masses can be compared with various experimental glueball candidates, providing a useful alternative to the conventional ELMC estimates.

Acknowledgements: SD thanks Prof. F. Lenz (Erlangen) and Mrs. van de Sande for hospitality during part of the work, and M. Teper for many helpful interactions. The work of SD was supported by a Particle Physics and Astronomy Research Council (U.K.) Advanced Fellowship and a CERN fellowship.

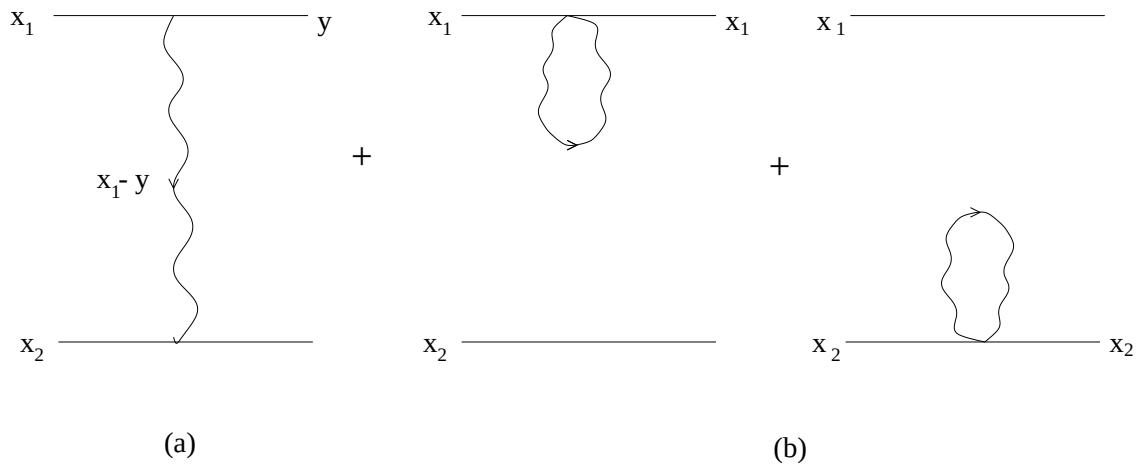

Figure 16: (a) Coulomb exchange graph; (b) self-energy graphs (contraction of (a).

A A_- Zero Modes

In this appendix, we argue that the only effect of the A_- zero modes c_i in the longitudinal Coulomb interaction (27) is to finitely renormalise the link field mass μ^2. The two processes contributing to Coulomb exchange between link-variables $M_r(\mathbf{x})$ in light-front Hamiltonian bound state equations are shown diagrammatically in Fig. 16 (see for example Refs. [22] for further discussion). Fig. 16(a) represents the instantaneous exchange of the A_+ non-zero mode, while Fig. 16(b) is the self-energy contribution arising from normal-ordering the former. Neglecting c_i, Fig. 16(b) acts to regulate the singular behaviour of Fig. 16(a) at zero momentum transfer, by an equivalent principle value prescription [2]. Let us denote the relevant Fock wavefunction of the two link variables by $f(\cdots, x_1, x_2, \cdots)$ (or $f(x_1, x_2)$ for short), for neighboring links in the colour Trace of a string state (e.g.39), carrying momenta x_1P^+ and x_2P^+ in the boundstate $|\Psi(P^+)\rangle$ of total momentum P^+. As explained in section 3.5, only neighboring links in the colour Trace have Coulomb exchange interactions in the large-N limit. We can neglect labels for the link variables other than longitudinal momentum. Our basic assumption in the following is that in order to estimate the effect of zero modes c_i, which are constrained variables at large N whose distribution $\phi(c_1, \ldots, c_N)$ is in principle known, we insert a c-number $C/\mathcal{L}$ wherever a quantity like $c_i/\mathcal{L}$ would appear in the exact expression at finite $\mathcal{L}$. In particular, C's appearing in any expression should not be identified numerically with one another, but each represent something $O(1)$ in the continuum limit $\mathcal{L} \to \infty$.

The contribution of the Coulomb interaction to the matrix element of the light-front Schrödinger

operator $\langle \mathrm{Fock}|2P^+P^-|\Psi\rangle$ is of the form[8]

$$I(x_1,x_2) = \mathcal{L}\sum_{m=1}^{n_1+n_2}\frac{n_1+m+C}{\sqrt{(n_1+C)(m+C)}}\frac{1}{(n_1-m+C)^2} \cdot\left\{\frac{f(n_1,n_2)(n_1+m+C)}{\sqrt{(n_1+C)(m+C)}}-\frac{f(m,n_1+n_2-m)(2n_2+n_1-m+C)}{\sqrt{(n_2+C)(n_1+n_2-m+C)}}\right\}. \quad (105)$$

Here $x_1 = n_1/K$, $x_2 = n_2/K$, and $n_1, n_2, m \neq n_1$ are non-zero integers less than integer $K = \mathcal{L}P^+/2\pi$. (If we could set $C = 0$ and take the limit $\mathcal{L}\to\infty$, we would recover the naive kernel of Ref. [2], which employed the naive light-front gauge $A_- = 0$.) For a finite free kinetic energy in the colour-dielectric regime, n_1 and n_2 must be both $O(\mathcal{L})$. We Taylor expand (105) in $C/\mathcal{L}$ to obtain

$$\begin{aligned} I(x_1,x_2) &= \mathcal{L}\sum_{m'=-n_1}^{n_2}\frac{2n_1+m'}{\sqrt{n_1(n_1+m')}}\frac{1}{(C-m')^2} \\ &\quad\cdot\left\{\frac{f(n_1,n_2)}{\sqrt{n_1(n_1+m')}}\left(2n_1+m'-C\left(1-\frac{(2n_1+m')^2}{n_1(n_1+m')}\right)\right)\right. \\ &\quad\left.-\frac{f(n_1+m',n_2-m')}{\sqrt{n_2(n_2-m')}}\left(2n_2-m'-C\left(1-\frac{(2n_2-m')^2}{n_2(n_2-m')}\right)\right)\right\} \\ &\quad+O\left(\frac{C}{\mathcal{L}}\right). \end{aligned} \quad (106)$$

The higher corrections $O(C/\mathcal{L})$ can be dropped in the continuum limit. We consider first the term at $O(C)$ in the curly brackets of (106). As $\mathcal{L}\to\infty$ it can only affect the finite part of I through the region of infinitesimal momentum transfer $m' = m - n_1 \sim O(1)$. In this region it simplifies to

$$\mathcal{L}f(n_1,n_2)\left(\frac{C}{n_1}+\frac{C}{n_2}\right)\sum_{m'=-n_1}^{n_2}\frac{1}{(C-m')^2} \quad (107)$$

which, when folded with the appropriate distribution $\phi(c_1,\cdots,c_N)^2$, is equivalent to shifting the mass μ^2 in boundstate equations. The key point is the absence of cross-terms like $1/\sqrt{x_1x_2}$. To actually calculate the mass shift would require ϕ, which we have not tried to determine in detail. In the case of $SU(2)$ scalar matter, it should be possible numerically to check whether the result of Ref. [21] can be reinterpreted as a mass shift. Note that our argument does not lead to any mass shift for fermionic matter.

Turning to the term $O(C^0)$ in the curly brackets of (106), this reduces to the continuum kernel of Ref. [2] but for the contributions in the region $m' \sim O(1)$. To discuss the latter, we must specify more carefully the C's. The correct expression for this region is (c.f. (31))

$$\int_0^1 dc_i\,|\phi(c_1,\cdots,c_N)|^2 4\,\Delta f(n_1,n_2)\,\mathcal{L}\sum_{m'=-n_1}^{n_2}\frac{m'}{(c_i-c_j-m')^2}+O(1/\mathcal{L}) \quad (108)$$

[8]Here we neglect to show mass renormalisations which are known already from the naive analysis [3].

where we have now explicitly integrated over the zero mode distribution ϕ, and used

$$f(n_1, n_2) - f(n_1 + m', n_2 - m') = m' \, \Delta f(n_1, n_2) + O(1/\mathcal{L}^2) \tag{109}$$

with $\Delta f(n_1, n_2) \sim O(1/\mathcal{L})$. At first sight it appears as if the zero modes c_i spoil the cancellation of (108) between positive and negative m' which would occur in their absence. However, using the fact that ϕ has definite symmetry under interchange of any two c_i's, ones sees that after integration over c_i's, the cancellation does hold. Another, more physical, way to see why this cancellation must occur, is that a derivative term $df(x)/dx$ would result in the continuum bound state equation if it did not. Such a term would violate $x^{D-1} \to -x^{D-1}$ symmetry in general.

B Nonzero winding and nonzero transverse momentum

The analysis of nonzero transverse momentum in Section 7.1 can be extended to nonzero winding number $\mathbf{n} \neq 0$. Thus one can also study the Lorentz boost properties of the winding modes (we have not yet attempted systematic study of this).

Let us start with a p-link state that winds once around a lattice with $\mathbf{n}$ transverse links. A generic $\mathbf{P} = 0$ state has the form

$$\begin{aligned} \big|\Psi(P^+, 0)\big\rangle = \frac{1}{\sqrt{V N^p}} \sum_{\mathbf{y}} \mathrm{Tr}\Big\{ & a^\dagger_{\lambda_1}(k_1, \mathbf{x}_1 + \mathbf{y}) a^\dagger_{\lambda_2}(k_2, \mathbf{x}_2 + \mathbf{y}) \\ & \cdots a^\dagger_{\lambda_p}(k_p, \mathbf{x}_p + \mathbf{y}) \Big\} \, |0\rangle \end{aligned} \tag{110}$$

where $\mathbf{y}$ is summed over all $V = n^1 \cdots n^{D-2}$ sites of the lattice and $\sum_i \widehat{\lambda}_i = \mathbf{n}$. By periodicity of the lattice we identify $a^\dagger_\lambda(k, \mathbf{x})$ with $a^\dagger_\lambda(k, \mathbf{x} + a\mathbf{n})$. The transverse coordinates are given by the formula

$$\mathbf{x}_i = \mathbf{x}_{i-1} + a \, \widehat{\lambda}_{i-1} \, , \quad 1 < i \leq p \, . \tag{111}$$

Note that the number of nonzero contractions $w = \langle \Psi(P^+, 0) | \Psi(P^+, 0) \rangle$ must divide n^r evenly, $n^r / w \in \mathcal{Z}$, for all r. Now, we will boost this state (110) to some finite transverse momentum $\mathbf{P}$:

$$\begin{aligned} \big|\Psi(P^+, \mathbf{P})\big\rangle &= \mathrm{e}^{i P^r M_{-r}/P^+} \big|\Psi(P^+, 0)\big\rangle \\ &= \frac{1}{\sqrt{V N^p}} \sum_{\mathbf{y}} \mathrm{e}^{i\mathbf{P}\cdot\mathbf{y}} \, \mathrm{Tr}\Big\{ a^\dagger_{\lambda_1}(k_1, \mathbf{y}) a^\dagger_{\lambda_2}(k_2, \mathbf{x}_2 + \mathbf{y}) \cdots a^\dagger_{\lambda_p}(k_p, \mathbf{x}_p + \mathbf{y}) \Big\} \, |0\rangle \ . \end{aligned} \tag{112}$$

For nonzero winding, the phase condition introduced earlier (77) has no particular advantage; instead we have chosen the convention $\mathbf{x}_1 = \bar{\mathbf{x}} = 0$.

Since we have a periodic lattice, $\mathbf{P}$ can only take on discrete values

$$l^r \equiv \frac{a P^r n^r}{2\pi} \in \mathcal{Z} \quad \text{(no sum over } r\text{)}. \tag{113}$$

We find the inner product

$$\begin{aligned}\langle\Psi(P^+,\mathbf{P})|\Psi(P^+,\mathbf{P})\rangle &= \langle\Psi(P^+,0)|\,\mathrm{e}^{-iP^rM_{-r}/P^+}\mathrm{e}^{iP^rM_{-r}/P^+}\,|\Psi(P^+,0)\rangle \\ &= \sum_{v=0}^{w-1}\mathrm{e}^{ia\mathbf{P}\cdot\mathbf{n}v/w} \\ &= \begin{cases} w\,, & \sum_r l^r/w\in\mathcal{Z} \\ 0\,, & \text{otherwise}\end{cases}\quad . \end{aligned} \tag{114}$$

Thus, as we change the transverse momentum, the number of states in a basis can change. Unlike the $\mathbf{n}=0$ case, the boost operator is no longer self-adjoint due to the finite transverse volume of the system.

In practical calculations, we prefer to work with real numbers. Thus, we introduce orientation reversals

$$\begin{aligned}&\mathcal{O}\,\mathrm{Tr}\Big\{a^\dagger_{\lambda_1}(k_1,\mathbf{x}_1)a^\dagger_{\lambda_2}(k_2,\mathbf{x}_2)\cdots a^\dagger_{\lambda_p}(k_p,\mathbf{x}_p)\Big\}\,|0\rangle \\ &\quad= \mathrm{Tr}\Big\{a^\dagger_{\lambda_p}(k_p,\mathbf{y}_1)a^\dagger_{\lambda_{p-1}}(k_{p-1},\mathbf{y}_2)\cdots a^\dagger_{\lambda_1}(k_1,\mathbf{y}_p)\Big\}\,|0\rangle\ . \end{aligned} \tag{115}$$

We perform no cyclic permutations on the colour trace. We find

$$\mathbf{y}_i = \mathbf{n}-\mathbf{x}_{p-i+1} \tag{116}$$

Consequently, $\mathcal{O}\,\mathrm{e}^{iB}\,\mathcal{O}=\mathrm{e}^{-iB}$ where $B=P^rM_{-r}/P^+$. It is useful to introduce the two states:

$$\begin{aligned}|A(P^+,\mathbf{P})\rangle &= \cos(B)\,(1+\mathcal{O})|\Psi(P^+,0)\rangle \\ |B(P^+,\mathbf{P})\rangle &= \sin(B)\,(1-\mathcal{O})|\Psi(P^+,0)\rangle\ . \end{aligned} \tag{117}$$

For states without symmetry under orientation reversal $\langle\Psi(P^+,0)|\mathcal{O}|\Psi(P^+,0)\rangle=0$, we find the inner products

$$\langle A(P^+,\mathbf{P})|A(P^+,\mathbf{P})\rangle = \langle B(P^+,\mathbf{P})|B(P^+,\mathbf{P})\rangle = \begin{cases} w\,, & \sum_r l^r/w\in\mathcal{Z} \\ 0\,, & \text{otherwise}\end{cases} \tag{118}$$

$$\langle A(P^+,\mathbf{P})|B(P^+,\mathbf{P})\rangle = \langle B(P^+,\mathbf{P})|A(P^+,\mathbf{P})\rangle = 0 \tag{119}$$

For states which are symmetric under orientation reversal $\langle\Psi(P^+,0)|\mathcal{O}|\Psi(P^+,0)\rangle\neq 0$, $|A(P^+,\mathbf{P})\rangle$ and $|B(P^+,\mathbf{P})\rangle$ are equivalent up to a phase factor. In this case, we include only the $|A(P^+,\mathbf{P})\rangle$ state in the basis. Occasionally, $\langle A(P^+,\mathbf{P})|A(P^+,\mathbf{P})\rangle=0$ in which case we include $|B(P^+,\mathbf{P})\rangle$ in the basis instead.

C Improved matrix elements for DLCQ

In this section, we will describe some refinements to the basic technique introduced in Appendix C of **I**. Our method is the following: when calculating the matrix elements of the Hamiltonian in a

many-particle calculation, we will use ordinary DLCQ commutation relations to calculate contractions associated with spectator particles. To calculate the interaction itself, we take the DLCQ momenta of the interacting particles, project onto a smooth wavefunction basis (continuous longitudinal momentum), and calculate matrix elements of the interaction in this smooth wavefunction basis. Our modification of DLCQ essentially eliminates the $1/\sqrt{K}$ and $1/K^{2\beta}$ errors associated with small momenta. The remaining errors include a (small) $1/K$ error from the instantaneous interaction $1/(k^+ - p^+)^2$, $1/K^2$ errors from DLCQ itself, and a $1/K$ error from production of particles at small momentum. In the following, we discuss improvements to the (2 particles) $\to$ (2 particles) interactions, the (1 particle) $\to$ (3 particles) interactions, and the heavy source interactions. The 'particles' in the present context are the link fields of course.

C.1 (2 particles) $\to$ (2 particles) interactions

Consider a typical 4-point interaction

$$V\left(\frac{k_1}{K}, \frac{k_3}{K}\right) = \quad (120)$$

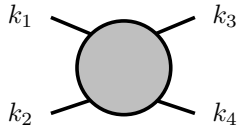

with DLCQ momenta $k_i \in \{1/2, 3/2, \ldots\}$ and $K = k_1 + k_2 = k_3 + k_4$. In particular, the mass term is treated as if it were a 4-particle interaction:

$$V(x,y) = \frac{\mu^2}{2}\left(\frac{1}{x} + \frac{1}{1-x}\right)\delta(x-y)\ . \quad (121)$$

We start by calculating eigenfunctions of the two-particle bound state equation [2].

$$\begin{aligned} &\mathcal{M}^2 f(x,1-x) \\ &= \int_0^1 dy\, H(x,y)\, f(y,1-y) \\ &= \frac{\mu^2\, f(x,1-x)}{x(1-x)} - \frac{G^2 N}{4\pi}\int_0^1 dy\, \frac{f(y,1-y)}{\sqrt{x(1-x)y(1-y)}}\left(\frac{(x+y)(2-x-y)}{(x-y)^2} + 1\right) \end{aligned} \quad (122)$$

where $\lambda_1 + \lambda_2/2 + \lambda_3 = -G^2 N a^{D-2}$. Then we write the incoming and outgoing DLCQ states as linear combinations of the first K eigenfunctions and evaluate matrix elements of the various interactions $V(x,y)$ in the eigenfunction basis.

We introduce a basis of even and odd wavefunctions (labeled by subscripts s and s'):

$$\phi_s(x) = (x(1-x))^\beta \begin{cases} \cos\left(\pi s\left(x-\frac{1}{2}\right)\right)\ , & s \in \{0,2,\ldots,2S\} \\ \sin\left(\pi s\left(x-\frac{1}{2}\right)\right)\ , & s \in \{1,3,\ldots,2S-1\} \end{cases}\ , \quad (123)$$

with β is given by $\mu^2 = G^2 N \beta \tan(\pi\beta)$, $0 < \beta < 1/2$. We define, for both even and odd wavefuntions, matrix elements of the various interaction terms $V_{s,s'} = \int dx\, dy\, \phi_s(x)\, V(x,y)\, \phi_{s'}(y)$,

the inner product matrix $E_{s,s'} = \int dx\, dy\, \phi_s(x)\, \phi_{s'}(y)$, and the two-particle Hamiltonian $H_{s,s'} = \int dx\, dy\, \phi_s(x)\, H\,(x,y)\ \phi_{s'}(y)$. In addition, we define the matrix $T_{i,s}$ which maps the wavefunction basis onto the DLCQ basis

$$T_{i,s} = \left(\frac{k_1 k_2}{K^2}\right)^{\beta} \left\{ \begin{array}{l} \cos\left(\pi s\left(\frac{k_1-k2}{2K}\right)\right) \\ \sin\left(\pi s\left(\frac{k_1-k2}{2K}\right)\right) \end{array} \right. \tag{124}$$

where the subscript $i \in \{1, 2, \ldots K\}$ denotes a two particle DLCQ basis state with momenta $k_1 = i - 1/2$, $k_2 = K - k_1$.

This choice of basis wavefunctions has several advantages over our previous choice. First, this basis is numerically 'well-conditioned' while the previous choice was numerically unstable. Second, the highly excited eigenfunctions of (122) are themselves nearly sines and cosines. We now generate the improved matrix elements at the beginning of a calculation, store them in memory, and use them as needed.

One calculates the various integrals using the formula

$$\int_0^1 dx\, x^\mu (1-x)^\mu\, \cos\left(2a\,(x-1/2)\right) = \sqrt{\pi}\,\Gamma(\mu+1)\, f_{\mu+1/2}(2a) \tag{125}$$

where $f_\mu(x)$ is defined in terms of a Bessel function:

$$\begin{aligned} f_\mu(z) &= J_\mu(z/2)/z^\mu & (126)\\ \frac{d}{dx} f_\mu(x) &= -\frac{x}{2} f_{\mu+1}(x) & (127)\\ 4\mu f_\mu(x) &= f_{\mu-1}(x) + x^2 f_{\mu+1}(x) & (128)\\ \lim_{x\to 0} f_\mu(x) &= \frac{1}{\Gamma(\mu+1)2^{2\mu}}\ . & (129) \end{aligned}$$

Thus, for example,

$$E_{s,s'} = \frac{\sqrt{\pi}}{2}\,\Gamma(2\beta+1)\left[f_{2\beta+\frac{1}{2}}\left(\pi(s-s')\right) \pm f_{2\beta+\frac{1}{2}}\left(\pi(s+s')\right)\right]\ . \tag{130}$$

The greatest difficulty comes from the instantaneous interaction

$$V_{s,s'} = -\frac{G^2 N}{8\pi}\int dx\, dy\, \frac{(x+y)(2-x-y)\,\phi_s(x)\,\phi_{s'}(y)}{\sqrt{xy(1-x)(1-y)}(x-y)^2}\ . \tag{131}$$

We cannot solve this integral analytically, but we can subtract the pole part at $x = y$ and solve the remaining finite integral numerically. Thus, we add and subtract the quantity

$$\begin{aligned} -\frac{G^2 N}{8\pi}\int dx\, dy\, &\frac{(x+y)(2-x-y)\,(x(1-x)y(1-y))^{\beta-1/2}}{(x-y)^2} \\ &\cdot\left[\frac{1}{2}\cos\left[\frac{\pi}{2}(s-s')(x+y-1)\right] \pm \frac{1}{2}\cos\left[\frac{\pi}{2}(s+s')(x+y-1)\right]\right] \end{aligned} \tag{132}$$

which, using the identity

$$\frac{1}{(x-y)^2} = -\lim_{\epsilon\to 0}\int_0^\infty dz\, z\cos(z(x-y))\ \mathrm{e}^{-\epsilon z}\ , \tag{133}$$

equals

$$\begin{aligned} G^2N\frac{\Gamma(\beta+1/2)}{16}\Big\{ & f_\beta\big(v^-\big)\left[(1+4\beta)\,f_\beta\big(v^-\big) - 2\left(v^-\right)^2 f_{\beta+1}\big(v^-\big)\right] \\ & \pm f_\beta\big(v^+\big)\left[(1+4\beta)\,f_\beta\big(v^+\big) - 2\left(v^+\right)^2 f_{\beta+1}\big(v^+\big)\right]\Big\} \end{aligned} \tag{134}$$

where $v^\pm = \pi(s\pm s')/2$. The numerical integration of (131) minus (132) is performed using the Gauß-Jacobi method [32] which correctly handles the endpoint behavior of the integrand and converges exponentially fast.

We solve the generalised eigenvalue problem $H\chi_t = h_t E\chi_t$ where the eigenvectors χ_t have normalisation $\chi^\dagger_{t'}E\chi_t = \delta_{t,t'}$. Using the lowest K eigenvectors, we define an eigenstate basis (denoted by subscripts t and t'),

$$T_{i,t} = T_{i,s}\,(\chi_t)_s\ . \tag{135}$$

To make the transformation between the DLCQ and eigenfunction bases orthonormal, we perform a standard QR-factorisation [32], $T_{i,t} = Q_{i,t'}R_{t',t}$, and discard the triangular matrix R (diagonal elements of R must be positive). Finally, we define the improved matrix elements by

$$V_{i,j} = Q_{i,t}\,(\chi_t)^\dagger_s\,V_{s,s'}\,(\chi_{t'})_{s'}\,Q^T_{t',j}\ . \tag{136}$$

C.2 (1 particle) → (3 particles) interactions

From the general bound state equations of two-dimensional gauge theories with pair production, one can show that as the momenta of any *two* particles go to zero the wavefunction becomes constant [31]. Thus we define a basis of wavefunctions

$$\phi_{k_1,k_2,k_3}(x,y) = C_{k_1,k_2,k_3}\begin{cases} \dfrac{(xy(1-x-y))^\beta}{((x+y)(1-x)(1-y))^{2\beta}}\ , & (x,y)\in R_{k_1,k_2,k_3} \\ 0\ , & \text{otherwise}\end{cases}\ . \tag{137}$$

with normalisation

$$1 = \int_0^1 dx\int_0^{1-x} dy\,\phi_{k_1,k_2,k_3}(x,y)^2 \tag{138}$$

for three outgoing particles with longitudinal momentum fractions x, y, and $1-x-y$ in the continuous wavefunction basis and $k_i \in \{1/2, 3/2, \ldots\}$, $K = k_1+k_2+k_3$, in the DLCQ basis. We define the polygonal region R_{k_1,k_2,k_3} surrounding $(k_1/K, k_2/K)$ as shown in Fig. 17.

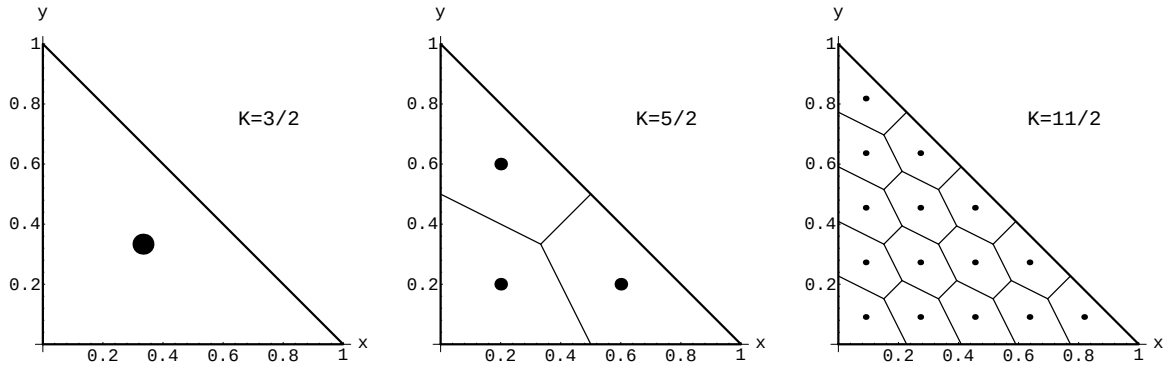

Figure 17: Region R_{k_1,k_2,k_3} for $K = 3/2$, $K = 5/2$, and $K = 11/2$. The dots represent the points $(k_1/K, k_2/K)$ and R_{k_1,k_2,k_3} is the surrounding polygonal region.

Consider a typical 4-point interaction

$$V\left(\frac{k_1}{K}, \frac{k_2}{K}, \frac{k_3}{K}\right) = K \quad . \tag{139}$$

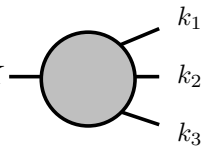

We calculate improved matrix elements associated with interaction $V(x, y, 1-x-y)$ using the expression

$$V_{k_1,k_2,k_3} = \int_0^1 dx \int_0^{1-x} dy\, \phi_{k_1,k_2,k_3}(x,y) V(x,y,1-x-y) \; . \tag{140}$$

The integrals are calculated numerically, paying careful attention to the small momentum regions.

C.3 Heavy source interactions

Improvement of the matrix elements for the interactions between the heavy sources and the link fields is particularly challenging because of the oscillatory nature of the wavefunction for large separation L and the presence of the cutoff $P_{\max}$. So far, we have concentrated on removing the leading errors which are, as before, associated with small longitudinal momenta and are of order $1/(K_{\max})^{2\beta}$ and $1/\sqrt{K_{\max}}$. At this point it makes no sense to include the finite L phase factors in the improvement scheme because we will also neglect oscillation of the wavefunction itself in the improved matrix elements. The leading error associated with the improved matrix elements is of order $1/K_{\max}$.

For (source-link) $\to$ (source-link) interactions, we define wavefunctions

$$\phi_k(x) = C_k \begin{cases} x^\beta \; , & k - 1/2 < x < k + 1/2 \\ 0 \; , & \text{otherwise} \end{cases} \tag{141}$$

where $k, k' \in \{1/2, 3/2, \ldots\}$, restricted by $K_{\max} \geq K_{\text{link}}$, is the DLCQ momentum of the link field neighboring the heavy source and x is its continuum longitudinal momentum rescaled by

$K_{\max}/(v^+\sqrt{G^2N}P_{\max})$. The normalisation is $1 = \int dx\,\phi_k(x)^2$. We calculate improved matrix elements for the various interactions using

$$V_{k,k'} = \int dx\,dy\,\phi_k(x)\,V(x,y)\,\phi_{k'}(y) \tag{142}$$

with the finite L phase factor replaced by its DLCQ value

$$\exp\left(\frac{iL\sqrt{G^2N}(x-y)P_{\max}}{2K_{\max}}\right) \to \exp\left(\frac{iL\sqrt{G^2N}(k-k')P_{\max}}{2K_{\max}}\right) . \tag{143}$$

In the case of the mass term for the link field adjacent to the heavy source, we assign half of the contribution to the link-link interactions acting on the interior of the string, consistent with Eqn. (121), and the other half to the heavy-link interaction. Thus, we use

$$V(x,y) = \frac{\mu^2 K_{\max}}{2x\sqrt{G^2N}P_{\max}}\,\delta(x-y) . \tag{144}$$

For the instantaneous A_+ exchange interaction, we must be careful about how we handle the $1/(x-y)^2$ pole and the $K_{\max} \geq K_{\text{link}}$ cutoff. For the off-diagonal part, we use

$$V_{k,k'} = -\frac{\sqrt{G^2N}K_{\max}}{8\pi(k-k')^2P_{\max}}\exp\left(\frac{iL\sqrt{G^2N}(k-k')P_{\max}}{2K_{\max}}\right)\int dx\,dy\,\frac{x+y}{\sqrt{xy}}\,\phi_k(x)\,\phi_{k'}(y) , \quad k \neq k' . \tag{145}$$

If the $1/(x-y)^2$ pole were left inside the integral, there would be a logarithmic divergence when $k = k' \pm 1$. The diagonal part is obtained by adding and subtracting the 'self-inertia'

$$V_{k,k} = \sum_{k'\neq k}^{K_{\max}\geq K_{\text{link}}} |V_{k,k'}|\left(\frac{k'}{k}\right)^\beta - \frac{\sqrt{G^2N}K_{\max}}{8\pi P_{\max}}\int_0^{K'} dy\,\frac{k+y}{\sqrt{ky}\,(k-y)^2}\left(\frac{y}{k}\right)^\beta \tag{146}$$

where $K' = K_{\max} - K_{\text{link}} + k$. The integral is solved numerically with an implicit principle value prescription for the pole at $y = k$. This method for handling the self-inertias is discussed in Ref. [33].

Turning our attention to the (source) $\to$ (source + 2 links) interactions, we proceed in an analogous manner. Since the wavefunction becomes constant as any two momenta go to zero, we define wavefunctions

$$\phi_{k_1,k_2}(x,y) = C_{k_1,k_2}\begin{cases} \dfrac{(xy)^\beta}{(x+y)^{2\beta}} , & k_1 - 1/2 < x < k_1 + 1/2 \text{ and} \\ & k_2 - 1/2 < y < k_2 + 1/2 \\ 0 , & \text{otherwise} \end{cases} \tag{147}$$

where $k_1, k_2 \in \{1/2, 3/2, \ldots\}$ are the DLCQ momenta of the two outgoing link fields created adjacent to the source. The normalisation is $1 = \int dx\,dy\,\phi_{k_1,k_2}(x,y)^2$. We calculate improved matrix elements for the various interactions using

$$V_{k_1,k_2} = \int dx\,dy\,\phi_{k_1,k_2}(x,y)\,V(x,y) . \tag{148}$$

As before, the finite L phase factors in $V(x,y)$ are replaced by their DLCQ values.

References

[1] S. Dalley and B. van de Sande, Nucl. Phys. **B53** (Proc. Suppl.), 827 (1997); Phys. Rev. **D56**, 7917 (1997).

[2] W. A. Bardeen and R. B. Pearson, Phys. Rev. D **14**, 547 (1976).

[3] W. A. Bardeen, R. B. Pearson, and E. Rabinovici, Phys. Rev. D **21**, 1037 (1980).

[4] G. Mack, Nucl. Phys. **B235**, 197 (1984);
H. B. Nielsen and A. Patkos, Nucl. Phys. **B195**, 137 (1982);
H.-J. Pirner, Prog. Part. Nucl. Phys. **29**, 33 (1992).

[5] S. J. Brodsky, Lectures at the NuSS, Korea (1997), preprint SLAC-PUB-7645, `hep-ph/9710288`.

[6] G. 't Hooft, Nucl. Phys. **B72**, 461 (1974); Nucl. Phys. **B75**, 461 (1974).

[7] M. Burkardt, Phys. Rev. **D54**, 2913 (1996).

[8] M. Teper, preprint OUTP-98-29P, `hep-lat/9804008`.

[9] S. Dalley and T. R. Morris, Int. Journal Mod. Phys. **A5**, 3929 (1990).

[10] M. Burkardt and B. Klindworth, Phys. Rev. D **55**, 1001 (1997).

[11] K. G. Wilson, Phys. Rev. D **10**, 2445 (1974).

[12] P. A. Griffin, Nucl. Phys. **B139**, 270 (1992).

[13] D. Weingarten, Phys. Lett. **B90**, 220 (1980).

[14] K. G. Wilson, in *Recent Developments of Gauge Theories*, eds. G. 't Hooft *et al.*, Plenum New York (1980).

[15] J. B. Kogut and L. Susskind, Phys. Rev. **D9**, 3501 (1974).

[16] H.-J. Pirner, J. Wroldsen, and M. Ilgenfritz, Nucl. Phys. **B294**, 905 (1987);
B. Grossman *et. al.*, Int. J. Mod. Phys. **A6**, 2649 (1991).

[17] V. A. Franke, S. A. Paston, and E. V. Prokhvatilov, preprint SPbU-IP-98-5, `hep-th/9803035`.

[18] A. Casher, Phys. Rev. **D14**, 452 (1976);
T. Maskawa and K. Yamawaki, Prog. Theor. Phys. **56**, 270 (1976).
C. Thorn, Phys. Lett. **70B**, 77 (1977).

[19] H.-C. Pauli and S. J. Brodsky, Phys. Rev. D **32**, 1993 and 2001 (1985).

[20] V. A. Franke, Yu. A. Novozhilov, and E. V. Prokhvatilov, Lett. Math. Phys. **5**, 239 (1981); *ibid* 437;
F. Lenz, M. Thies, S. Levit, and K. Yazaki, Ann. Phys. **208**, 1 (1991);
F. Lenz, H. W. L. Naus, M. Thies, Ann. Phys. **233**, 317 (1994);
H-C. Pauli, A. C. Kalloniatis, and S. Pinsky, Phys. Rev. D **52**, 1176 (1995).

[21] A. S. Mueller, A. C. Kalloniatis, H-C. Pauli, preprint FAU TP3-98/7, `hep-th/9803204`.

[22] S. Dalley and I. R. Klebanov, Phys. Rev. D **47**, 2517 (1993);
K. Demeterfi, I. R. Klebanov, and G. Bhanot, Nucl. Phys. **B418**, 15 (1994);
F. Antonuccio and S. Dalley, Nucl. Phys. B **461**, 275 (1996); Phys. Lett. **B 376**, 154 (1996).

[23] J. B. Kogut and L. Susskind, Phys. Rev. D **11**, 395 (1975).

[24] D. A. Soper, Nucl. Phys. **B53** (Proc. Suppl.), 69 (1997).

[25] T. Eguchi and H. Kawai, Phys. Rev. Lett. **48**, 1063 (1983).

[26] G. Bhanot, U. M. Heller, and H. Neuberger, Phys. Lett. **B113**, 47 (1982).

[27] C. B. Thorn, Phys. Rev. **D19**, 639 (1979); Phys. Rev. **D20**, 1435 (1979).

[28] E. Witten, in *Recent Developments of Gauge Theories*, eds. G. 't Hooft *et al.*, Plenum New York (1980).

[29] M. Lüscher, K. Symanzik, and P. Weisz, Nucl. Phys. **B173** 365 (1980).

[30] Q. Z. Chen, X. Q. Luo, S. H. Guo, and X. Y. Fang, Phys. Lett. **B348** 560 (1995).

[31] S. Dalley, preprint CERN-TH/98-114, `hep-th/9804024`.

[32] W. H. Press, B. P. Flannery, S. A. Teukolsky, and W. T. Vetterling, *Numerical Recipes*, Cambridge University Press (1989);
G. H. Golub and C. F. Van Loan, *Matrix Computations*, Johns Hopkins University Press (1983).

[33] B. van de Sande, Phys. Rev. D **54**, 6347 (1996).